Energy Transfer Dynamics in Collisions of Polar and Non-polar Gases with ω-Functionalized Self-Assembled Monolayers

Megan E. Bennett

A thesis submitted to the faculty of Virginia Polytechnic Institute and State University in partial fulfillment of the requirements for the degree of

MASTERS OF SCIENCE

in

Chemistry

John R. Morris, Chair
Mark Anderson
Gary Long
Diego Troya

Date: May 7, 2007
Blacksburg, Virginia

Keywords:
ω-Functionalized SAMs, Molecular Beam, Energy Transfer Dynamics

Energy Transfer Dynamics in Collisions of Polar and Non-polar Gases with ω-Functionalized Self-Assembled Monolayers

Megan E. Bennett

ABSTRACT

Molecular beam scattering experiments are used to investigate the extent of thermal accommodation of Ne, CD_4, ND_3, and D_2O in collisions with long chain CH_3, NH_2, and OH terminated self-assembled monolayers (SAMs) on gold. Surface rigidity, internal degrees of freedom of the impinging gas, and potential energy surface well depths have been explored as a way to predict the outcome of a gas-surface collision. Ne is used to assess the mechanical rigidity of the SAMs. The order of rigidity is $CH_3 < NH_2 \sim OH$. The NH_2 and OH terminated SAMs are more rigid due to the intermolecular hydrogen bonding structure at the gas-surface interface. Despite the hydrogen bonding nature of the NH_2 and OH terminated SAMs CD_4, ND_3, and D_2O are extensively thermally accommodated on the surfaces, therefore surface rigidity is no solely responsible for energy transfer dynamics. It was found that the number of degrees of freedom do not predict how extensively a gas will thermally accommodate on a surface capable of hydrogen bonding. A qualitative correlation between increasing potential energy well depths and the extent of thermal accommodation has been established as a result of these scattering experiments.

ACKNOWLEDGEMENTS

I would like to thank Dr. John Morris for his guidance, support, and encouragement during my graduate career. I would also like to thank Dr. Mark Anderson, Dr. Gary Long, and Dr. Diego Troya for their advice and encouragement.

I would also like to thanks the members of the Morris group (Wes Gordon, Larry Fiegland, Josh Uzarski, Erin Davis, Jessica Lu, Leslie Adamczyk, and Will Alexander). I extend a special thanks to the BEAM TEAM (Will and Jessica) for their help in conducting experiments, the analysis of results, and assistance in writing this thesis.

Finally, I would like to thank my parents. Without their continuous support, encouragement, and love this would not have been possible. Thank you for always supporting me.

Table of Contents

List of Figures

List of Tables

List of Abbreviations

SAM = Self-Assembled Monolayer

UHV = Ultra High Vacuum

RAIRS = Reflection Adsorption Infrared Spectroscopy

XPS = X-ray Photoelectron Spectroscopy

IS = Impulsive Scattering

TD = Thermal Desorption

TOF = Time-of-Flight

MS = Mass Spectrometry

RGA = Residual Gas Analyzer

Chapter 1

Introduction

Thesis Statement

The aim of this research is to provide a fundamental and detailed understanding of how properties of polar and non-polar organic surfaces affect the energy transfer dynamics when both gases capable of hydrogen bonding and non-hydrogen bonding are scattered from organic surfaces.

1.1 Motivation and Background

Organic compounds are prevalent in aerosol particles in the upper troposphere, and greatly impact atmospheric chemistry.[1-3] The organic aerosols present in the troposphere often undergo oxidation reactions to become functionalized with carboxylic acid, hydroxyl, amine, and aliphatic organic groups[4-8]. Little is known about the mechanisms that produce functionalized organic aerosols.[4-8] In addition to the presence of organic aerosols in the atmosphere, there are many gas phase molecules available to interact, or react, with the aerosols. These molecules include ammonia (the most prevalent gaseous base in the atmosphere), water, and methane.[7, 8] Despite numerous studies that report the presence of organic aerosols and various gases in the atmosphere, very little is known about how ambient gases react with organic aerosols.

The collisions between ambient gases and organic functionalized surfaces produce a number of possible events. These possible events are shown in Figure 1. The first channel, impulsive scattering, occurs when the incident gas molecule impinges on the organic surface and immediately recoils back into gas phase. In direct reactive scattering, the impinging gas collides with the surface once and a reaction occurs. The gas molecule then recoils back into the gas phase. Alternatively, the gas molecule could lose enough energy during the initial collision to become trapped on the surface through Van der Waals, hydrogen bonding, dipole-dipole, or other forces. In the event that the impinging gas molecule becomes trapped on the surface, the gas molecule could undergo one of several events. In trapping-desorption, the gas molecule thermally equilibrates with the surface, and desorbs back into the gas phase without reaction. The thermally equilibrated gas molecule could also diffuse into the bulk phase and remain there

for extended periods of time. Provided that both the impinging gas molecule and the surface have sufficient reactivity, the thermally equilibrated gas molecule could react with the surface to form new surface species. The reacted species could remain on the surface, or desorb into the gas phase.

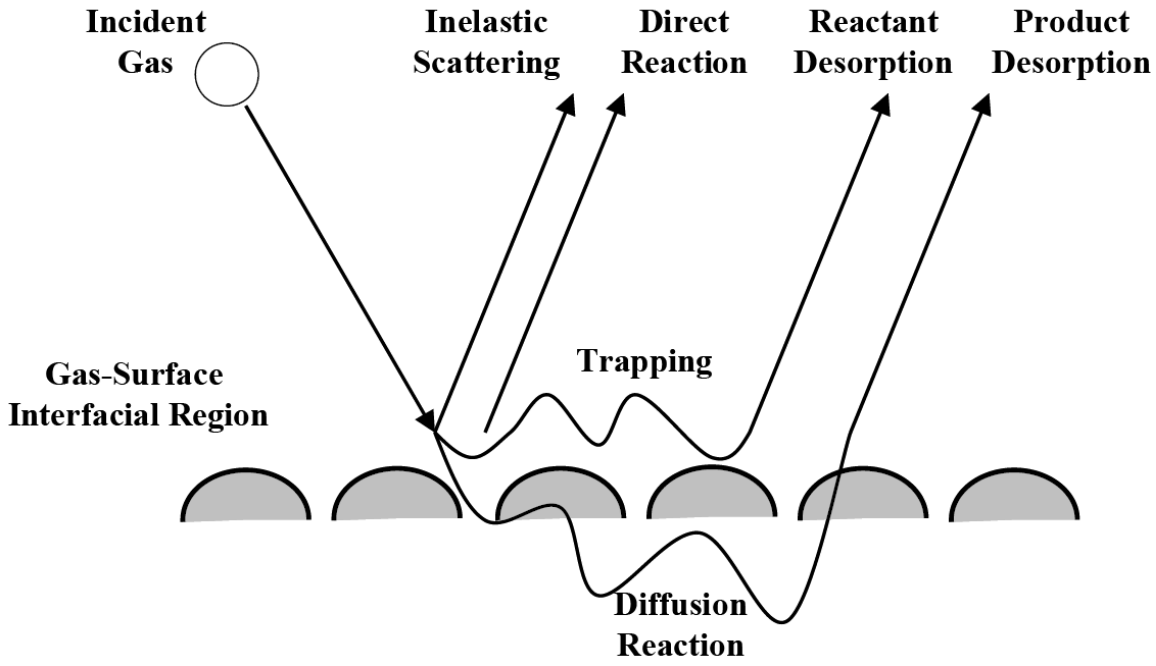

Figure 1. Possible events for an impinging gas molecule to interact with the surface.

The objective of this work is to provide a deeper understanding of how gas polarity and surface functionality affect gas-surface energy transfer dynamics. To study the energy transferred from an impinging gas molecule to the surface, molecular beam techniques, ultra-high vacuum (UHV) environments, and self-assembled monolayers (SAMs) are utilized. Molecular beam techniques are useful in the study of energy transfer dynamics because they provide a highly directional and nearly monoenergetic source of desired gaseous molecules. UHV is ideal for studying energy transfer dynamics due to virtual elimination of all gas-gas and gas-surface collisions. The elimination of gas-surface collisions allows for a clean environment. The surface will have a minute opportunity to be impinged on by gaseous molecules other than those in the molecular beam. The use of SAMs provides a highly-ordered, easily-characterized, and tunable surface. The properties of UHV environments, SAMs, and molecular beam techniques allow for investigation of energy transfer dynamics between a particular gas molecule and a specific functional group on a surface.

1.2 Recent Work in Atmospheric Gas-Surface Collisions

Nathanson and co-workers have recently scattered Ne, CH_4, NH_3, and D_2O from the liquid surfaces of squalane and glycerol.[9] The gases have similar sizes and masses, but have a range of chemical properties. The wide range of chemical properties and similar masses allow for the scattering dynamics to be attributed to the chemical properties of the gaseous species, not to kinematic effects. Nathanson and co-workers studied the energy transfer dynamics of the above gases and surfaces. The energy transfer dynamics were investigated through the use of time-of-flight techniques (TOF). The data showed two main scattering channels: impulsive scattering (IS) and thermal desorption (TD) (see Figure 1).

The results from the work of Nathanson et al. indicate that despite a variety of chemical properties of the gases, the energy transferred to the surface through the IS channel was similar in both the squalane and glycerol systems. However, Nathanson et al. did find significant differences in the fraction of molecules that thermally accommodated with the surface. They found that Ne and CH_4 accommodated more readily (had a higher TD energy transfer channel) on squalane than on glycerol. NH_3 accommodated slightly less on squalane than on glycerol, and D_2O accommodated best on glycerol. Based on these results, they concluded that energy transfer corresponds loosely with the solubility of molecules in the bulk phase, but that the energy transfer dynamics do not correspond directly to solubility. Henry's law solubility constants are indicative of how attracted a gas is to a bulk phase solvent, which could correspond to how attracted a gas is to a surface. The bulk Henry's law solubility constants and the TD fractions are shown in Table 1. One may predict Ne to accommodate approximately 10 times more readily on squalane than on glycerol based on Henry's law solubility constants. However, Nathanson and co-workers observed a TD fraction that is only five times greater for squalane. When Nathanson et al. scattered methane from the surfaces of squalane and glycerol, they observed a two-fold difference in the extent of thermal accommodation. Henry's law solubility constants predict that methane should accommodate six times greater on squalane than on glycerol. One may predict, based on solubility constants, that ammonia should accommodate far greater on glycerol than on squalane. However, Nathanson et al. reported a one percent difference in the extent of thermal accommodation between the two surfaces. Finally, when Nathanson and co-workers examined deuterated water scattering from the surfaces of squalane and glycerol, they found that deuterated water thermally accommodated twelve percent better on

glycerol. When examining solubility constants, one would expect water to accommodate far more readily on glycerol than on squalane. Overall, Henry's law solubility constants roughly allow for a qualitative prediction of gas-liquid energy transfer dynamics, but do not provide a quantitative prediction. It appears that the surface properties, rather than the bulk properties, play a major role in controlling the ability of a gas phase species to dissipate its energy to become thermally equilibrated on a surface.

Table 1. Henry's Law Solubilities and the TD fraction reported by Nathanson et al.

	Methanol Solubilities (χ_{soln} / P_{gas})	Alkanes Solubilities (χ_{soln} / P_{gas})	% TD $OH:CH_3$
Neon	$7.9X10^{-5}$	$3.5X10^{-4}$ (decane)	3 : 17
Methane	$8.6X10^{-4}$	$5.3X10^{-3}$ (decane)	15 : 33
Ammonia	0.31	$2.1X10^{-2}$ (hexadecane)	41 : 40
Water	22	$1.9X10^{-2}$ (hexane)	49 : 37

In addition to the above study, other investigations have been conducted on similar systems, to those used by Nathanson and co-workers. These studies may give insight into predicting gas-surface energy transfer dynamics. Recently, a number of studies have been conducted on the behavior of water with alcohols.[10-12] One of the studies found that at a neutral pH (7), the proton exchange probability for deuterated ethanol with water ranges from 3.3 % at 263 K to 5.1 % at 291 K. On the other hand, with lower or higher pH values, the exchange probability increases to between 14 and 18 percent.[13] Recent computational methods have revealed that water remains on the surface of glycerol for 0.5 ps, indicating that any proton exchange that could possibly occur between the OH group of glycerol and a proton from water would have to happen extremely rapidly.[10]

Recent work has also investigated polyatomic gases interacting with hydrogen bonding surfaces .[14-18] An investigation into systems of hydroxyl and carboxylic acid surfaces dosed with dimethylmethylphosphonate (DMMP) has shown that gases are capable of disrupting surface species that are strongly hydrogen bonding. When DMMP is dosed onto hydroxyl and carboxylic acid surfaces, the hydroxyl peak in the infrared spectrum shifts from 3330 cm^{-1} to 3440 cm^{-1}, and the carboxylate peak at 1718 cm^{-1} shifts to 1741 cm^{-1}. These findings indicate disordering of the hydrogen bonding network.[19] Temperature-programmed desorption studies have demonstrated that when the surface coverage of an alcohol increases, the energy needed to desorb the chains also increases. This phenomenon is likely due to the increased strength of the hydrogen bonding network and Van der Waals interactions between aliphatic groups of neighboring chains.[15] Valioka et al. have shown that SAMs containing amide groups establish a lateral hydrogen bonding network that stabilizes the SAMs thermally by 50 K, and increases the desorption energy by 7 kJ/mol.[20] In addition, Morris and co-workers have investigated the impact of surface functionality on gas-surface energy transfer dynamics. Rare gas scattering from methyl and hydroxyl terminated SAMs of similar chain length have shown that rare gases are better thermally accommodated, by 18 %, on the methyl terminated surface. The greater thermal accommodation of rare gases on methyl terminated surfaces indicate that the methyl surface is mechanically softer than the hydroxyl terminated surface.[16] The mechanical softness of the methyl terminated surface is likely due to the lack of the ability of aliphatic groups to hydrogen bond to one another. Morris et al. have also examined scattering of HCl from hydroxyl and methyl terminated SAMs.[16] It was reported that HCl experiences not only IS and TD channels, but is also capable of hydrogen bonding to the hydroxyl terminated SAM. The hydrogen bond between HCl and the OH group of the SAM is responsible for increased thermal accommodation probabilities, despite the increased rigidity of the hydroxyl surface relative to the methyl surface.

1.3 Summary and Research Goals

The fate of a gas molecule colliding with an organic surface is dependent upon the initial collision between the gas and the surface. Upon the initial collision of the gas with the surface, the gas molecule may impulsively scatter (impact the surface and immediately recoil into the gas phase), directly react with the surface and desorb into the gas phase, or become thermally

accommodated and possibly trapped on the surface. Gas molecules that are thermally accommodated on the surface can desorb into the gas phase or react with the surface (proton exchange). All of the channels are illustrated in Figure 1. The gas species, surface structure, and surface functionality all play a role in how energy is transferred from the gas to the surface.

The goal of this research is to further the understanding of gas-surface energy transfer dynamics, to explore the impact of surface structure and interfacial functionality, and determine the effect of the gas polarity on thermal accommodation. To attain this goal, UHV environment, molecular beams, and SAMs will be used. These techniques were chosen so that any event occurring on the surface can be attributed to only the gas-surface interactions. The specific research goals are 1) develop a fundamental understanding of the energy transfer of a gas-surface collision; 2) determine how surface structure and functionality effect thermal accommodation; 3) investigate how gas composition affects energy transfer and thermal accommodation. High energy molecular beams of Ne, CD_4, ND_3, and D_2O will be scattered from methyl, hydroxyl, and amine terminated monolayer surfaces, in order to achieve the goal of understanding gas-surface energy transfer dynamics.

Chapter 2

Experimental Approach

2.1 General Overview

Gas-surface chemistry reactions are initiated by the interactions of two single layers of molecules at the gas-surface interface. Understanding how a reaction is initiated can lead to the ability to predict how two reactants will interact with one another. Molecular beam techniques allow for the development of mechanistic understanding of the energy transfer dynamics at a gas-surface interface.

A nearly monoenergetic molecular beam is directed at the SAM in a UHV chamber. Upon contact with the self-assembled monolayer (SAM), the gaseous molecules from the molecular beam transfer a portion of their energy to the SAM. The interaction of each gaseous molecule that impinges on the surface may interact with the SAM differently. Differences in the gas-surface interaction leads to variances in energy transfer from the gas to the surface, thus creating a time-of-flight (TOF) distribution that is tracked using a mass spectrometer (MS).

The TOF can be calculated based on known energies of the molecular beam and known distances of the instrument. The distance from the chopper wheel to the surface, the distance from the surface to the MS, and the energy of the molecular beam are known. Therefore, the time it takes the molecular beam to reach the surface from the chopper wheel, and the time it takes the molecular beam to reach the MS after colliding with the surface can both be determined. The energy of the molecular beam before and after colliding with the surface can also be found. Comparison of the molecular beam energies before and after colliding with the surface allows for the amount of energy transferred from the molecular beam to the surface to be determined, thus giving insight into the mechanistic behavior of energy transfer at the gas-surface interface.

2.2 Self-Assembled Monolayers

2.2.1 Introduction

In order to study gas-surface interactions, one requires a well-ordered, reproducible structure with variable functionalization. SAMs fulfill these requirements. SAMs are most

commonly formed from alkanethiols. The sulfur group of the thiol chemisorbs to the substrate, in this case gold. The sulfur head group is attached to a carbon backbone that is attached to a functionalized tail group. The tail group is exposed at the gas-surface interface. This chemisorption of sulfur on to gold creates a dense monolayer (separation distance of ~5 Å), with a carbon chain tilt angle of ~30° from the surface normal. The packing density and tilt angle leads to a super lattice of (√30 x √30) R30°. SAMs have been shown to be stable in UHV environments for extended periods of time.[20-24]

2.2.2 Obtaining Alkanethiols

The alkanethiols used in these experiments are all commercially available. The 16-hexadecanethiol ($HS(CH_2)_{15}CH_3$), and the 16-hexadecan-1-olthiol ($HS(CH_2)_{16}OH$) were purchased from Aldrich, and used as received. The 11-aminoundecanethiol was obtained as the chloride salt ($HS(CH_2)_{11}NH_3^+Cl^-$) from Dojindo, and used as purchased to form a monolayer on gold. Once the protonated amine monolayer was formed it was rinsed with triethylamine (TEA), in order to remove the chloride ion and deprotonate the monolayer.

2.2.3 Preparation of the Monolayer

All SAMs used in this study were prepared by spontaneous chemisorption of the alkanethiol onto the gold substrate. The gold substrates used in this scattering study were purchased from Evaporated Metal Films Corporation (EMF), and consisted of 1mm thickness of glass with a 50 Å coating of titanium (as an adhesion layer), that was finished with a 1000 Å layer of 99.9 % gold. Before forming monolayers, the samples were cleaned in piranha solution (70 % concentrated sulfuric acid / 30 % of 30 % hydrogen peroxide) for approximately one hour. The samples were rinsed with copious amounts of deionized water and 200 proof ethanol after being removed from the piranha solution. Following rinsing, the samples were placed in an approximately one mM ethanolic solution of the desired thiol. After immersing the gold slide in the ethanolic solution for at least 24 hours, the methyl and hydroxyl terminated SAMs were rinsed with copious amounts of 200 proof ethanol. The slides were then dried with ultra-high purity nitrogen, mounted onto the sample mount, and transferred into the vacuum chamber. The sample containing the amino salt terminated SAM was additionally rinsed with copious amounts of triethylamine, in order to remove the chloride ion and deprotonate the salt. The sample was

then rinsed with 200 proof ethanol and dried with ultra high purity nitrogen, making the salt into an amine terminated SAM.

2.2.4 Surface Characterization

To establish how well-ordered the SAMs used in this study were, X-ray photoelectron spectroscopy (XPS) and reflection-adsorption infrared spectroscopy (RAIRS) were used. A Perkin-Elmer 5400 XPS with a 1253.6eV magnesium source was used for surface characterization of the 11-aminoundecane SAM. A Nicolet 710 nitrogen purge infrared spectrometer with RAIRS capability was used for the characterization of all the SAMs. From these surface characterization techniques, it was found that the methyl and hydroxyl terminated SAMs used in this study were well-ordered and similar in ordering to SAMs found in the literature. The amine terminated SAM was slightly disordered based on the RAIR spectrum.

2.3 Ultra-High Vacuum

A stainless steel chamber capable of maintaining ultra-high vacuum (UHV) conditions ($<10^{-9}$ torr) allows both the sample and the molecular beam to be nearly free of collisions with background gases. Background gases are those gases present in the chamber that are in addition to the gas molecules in the molecular beam). If the sample were to interact with background gases, the gases would contaminate the surface by changing the functionality or structure of the SAM. Surface contamination would hinder, if not eliminate, the ability to examine the desired gas-surface interaction. The lack of background gases virtually eliminates unwanted gas-gas collisions. Gas-gas collisions are undesirable because they change the trajectory and energy of the gas molecules in the molecular beam, both before and after the molecular beam collides with the surface. As a result, the ability to properly assess the interaction at the gas-surface interface is limited.

A schematic of the UHV chamber used in this study of gas-surface energy transfer dynamics can be seen in Figure 2. The SAM covered gold samples are initially placed in the load lock, which is quickly pumped down to approximately 10^{-6} torr, for about 30 minutes. The load lock allows for quick transfer of the surface samples into the main chamber without exposing the surface to atmospheric conditions for extended periods of time, and without compromising the UHV nature of the main chamber. The load lock is pumped with a turbomolecular pump (Pfeiffer TMU 071P pumping rate of $60 Ls^{-1}$).

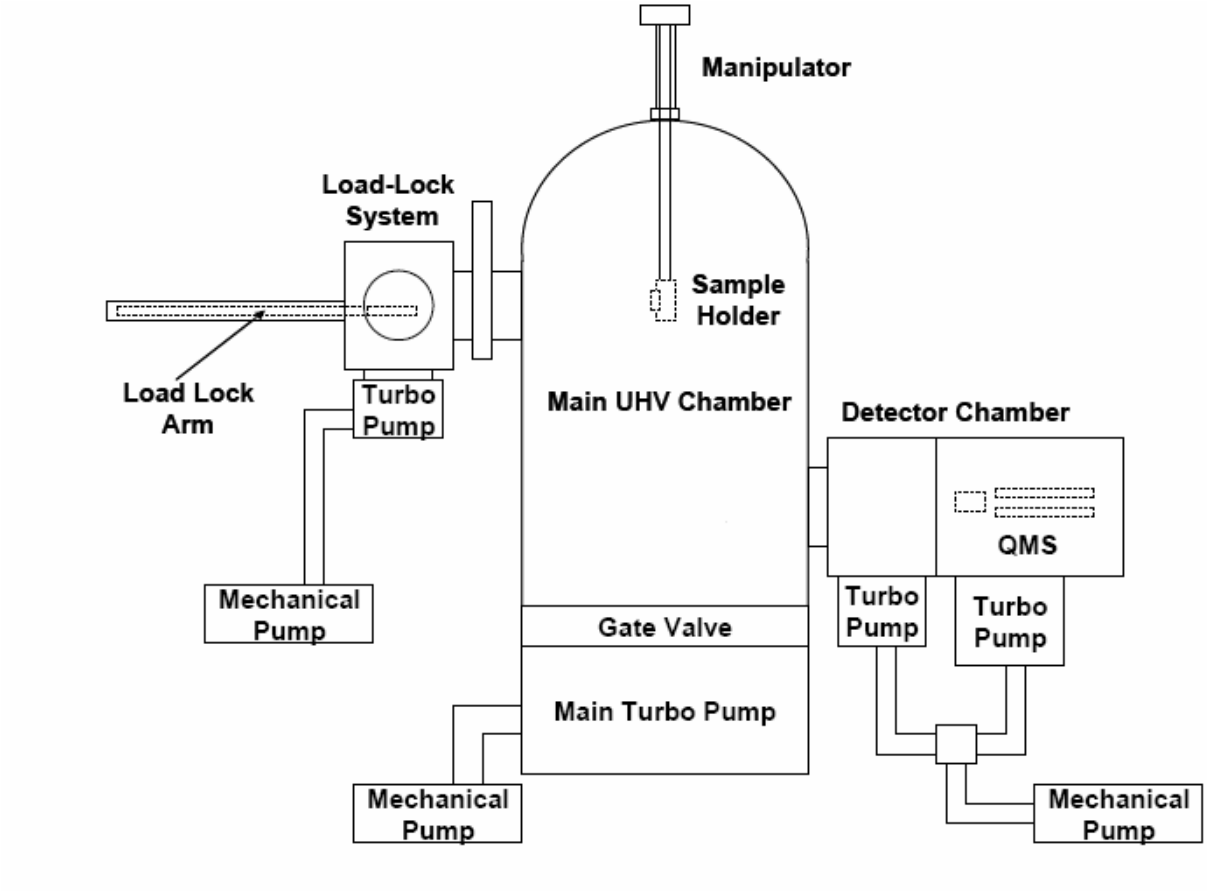

Figure 2. Schematic of the UHV chamber used for the study of gas-surface interfaces.

Once the load lock is pumped down to at least 10^{-6} torr, the samples are transferred into the main chamber through a gate valve using a sample transfer arm. The main chamber is pumped to a base pressure of approximately 2 x 10^{-9} torr by a large turbomolecular pump (Pfeiffer TMU 1601 pumping rate of 1500Ls^{-1}). Once the sample is transferred into the upper level of the main chamber the transfer arm is removed from the main chamber, and the gate valve is closed to seal the load lock chamber from the main chamber.

The sample is then lowered, via a motorized manipulator arm (McCallister, MA2012) into scattering position. Once lowered, the sample is aligned with the quadrapole mass spectrometer, ABB Extrel (MEXM 1000). The ABB Extrel is contained within two chambers that are differentially pumped. The first pumping stage, containing the ionizer, is separated from the

main chamber by a 4.3 mm aperture and is pumped on by a turbomolecular pump (Pfeiffer, TMU 261, pumping rate of 210 Ls^{-1}). The quadrapoles are also housed in the first differential pumping stage, separated from the ionizer by a 4.7 mm aperture. This differential pumping stage has a typical pressure of 3×10^{-10} torr. In addition to the ABB Extrel, there is a second mass spectrometer (SRS300 RGA) that is positioned in the main chamber, directly opposite the source chamber. The SRS RGA is directly in line with the molecular beam exiting the source chamber. The RGA is used for beam characterization.

Once the sample has been aligned with the ABB Extrel, the sample is rotated 30° using the precision manipulator arm, in order to align the sample with the molecular beam source. Alignment of the sample with the source is detailed in section 2.5.

2.4 Molecular Beam Sources

A molecular beam is a highly directional, tunable ray of gaseous molecules. The energy of a molecular beam is also tunable because the velocity of the gas is controllable. A molecular beam coupled with a UHV environment provides an excellent way to indirectly study gas-surface dynamics. Experimentally, it is extremely difficult to directly study the dynamics of the gas-surface interface. However, by studying the molecular beam before and after the gas molecules in the molecular beam collide with the surface, the dynamics of the gas-surface collision can be inferred. The UHV environment eliminates background gases from colliding with the surface and the beam, thus keeping the surface clean and maintaining the desired molecular beam properties. There are two kinds of molecular beams that can be used to study the dynamics of a gas colliding with a surface: an effusive beam and a supersonic beam. In the studies discussed here only a supersonic beam was used.

2.4.1 Supersonic Molecular Beam

A supersonic molecular beam is a highly direction, monoenergetic, and tunable ray of gas molecules. In a supersonic molecular beam, the pressure difference between the source and the surrounding vacuum chamber is large enough to draw the gas molecules out of the source aperture, and into the vacuum chamber. Forcing the molecules into the vacuum chamber is considered to be molecular flow, whereas effusive beams experience free-molecular flow. Upon exiting the source aperture, or nozzle, the centerline for the beam can reach speeds above Mach one.[25] Once the molecules are forced out of the source and into a vacuum chamber, the center of

the beam is extracted using an aperture that leads to a second vacuum chamber. In the center of the molecular beam, all the gas molecules have virtually the same velocities and do not interact with each other. Supersonic beams can be composed of pure gases or a mixture of gases.

Since mixtures of gases can be used, high energy molecular beams can be obtained (above 100 $kJmol^{-1}$). Mixtures of gases are made by seeding the heavier gas component in a lighter gas. This mixing allows the heavier gas to reach velocities close to those of the lighter gas. The lighter gas, or carrier gas, increases the velocity of the heavier gas. If a beam consists of two percent argon in helium mixture, the 98 percent of the beam that is helium accelerates the two percent argon in the beam to a higher velocity than the argon could achieve on its own. The properties of mixed high energy molecular beams are harder to calculate then those of an effusive molecular beam. Therefore, properties of supersonic molecular beams are determined by direct measurement, using such techniques as mass spectrometry. Figure 3 is a schematic of the supersonic molecular beam source used in these experiments.

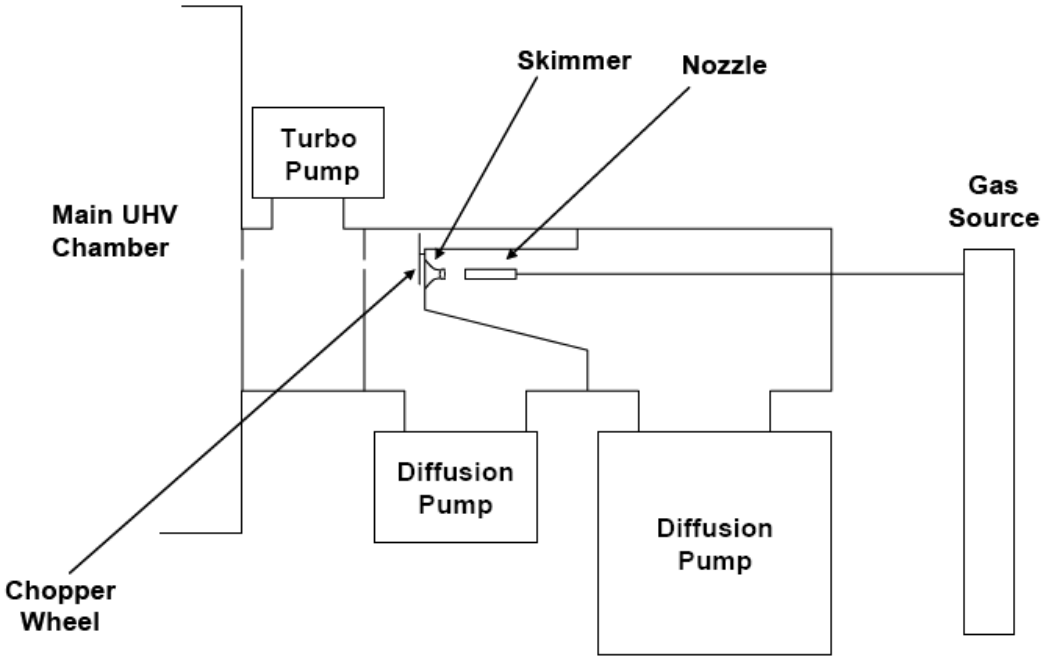

Figure 3. The supersonic source used in this study.

High energy molecular beams are created by expanding the seeded gas mixture through the source nozzle located in the first differential pumping stage that is pumped by a diffusion pump (VHS 10, Varian Vacuum Technologies, pumping speed of 5000 Ls^{-1}). The beam then passes through a 0.40 mm conical skimmer that extracts the center of the beam. After passing

through the conical skimmer, the beam enters the second differential pumping stage, pumped by a diffusion pump (Diffstak, MK2, BOC Edwards pumping speed of 1500 Ls^{-1}). The beam immediately collides with a chopper wheel rotating at 250 Hz in the second differential pumping stage. Upon colliding with the chopper wheel, the beam is chopped into short microsecond pulses. The beam then passes through a 1.5 mm colliminating skimmer before entering the final differential pumping stage, pumped by a turbo molecular pump (TMU 261P, Pfeiffer, pumping rate of 210 Ls^{-1}). At the final differential pumping stage, the molecular beam passes through a 2.2 mm aperture into the main chamber. The 2.2 mm aperture creates a 1.0 cm^2 beam spot on the surface sample 36 cm in front of the nozzle.

The molecular beam is characterized with a mass spectrometer (SRS RGA) located directly in front of and 44 cm from the nozzle. The schematic for beam characterization is illustrated in Figure 3. To characterize the beam, the translational arm holding the sample is raised out of the path of the molecular beam. Time-of-flight (TOF) data is then collected on the pulses of the molecular beam. From examining the arrival time of the pulses, the energy of the beam is determined.

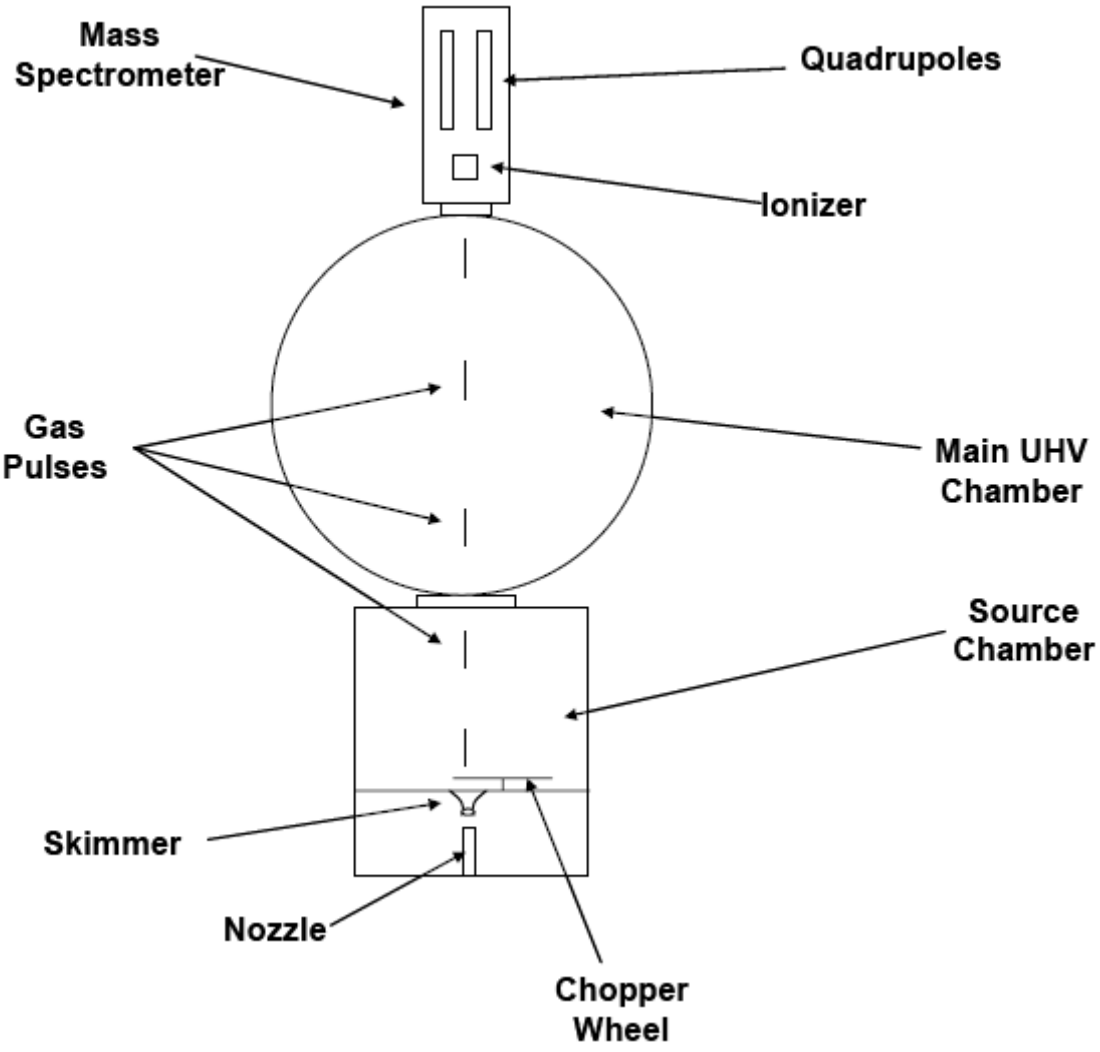

Figure 4. The schematic, as seen from above, for characterizing the beam energy.

2.5 Sample Positioning and Scattering

Once the sample mount, containing two surfaces, is placed in the load lock and the load lock reaches a pressure of 10^{-6} torr, the samples are transferred via a transfer arm into the main chamber. The main chamber has a base pressure of less than 2×10^{-9} torr. The samples enter the main chamber at a higher level than the scattering occurs at; therefore the samples are lowered to the scattering level (the Z direction) via a motorized manipulator arm. Once the surface samples have been lowered to the scattering level, one of the samples is aligned using a helium-neon (HeNe) laser located behind the main mass spectrometer. The laser shines through the quadrupole rods, an aperture, focusing lenses, an ionizer, and through a second aperture into

the main chamber where it intersects the desired sample. Once the laser beam intersects the sample, the tilt angle and angle of the sample mount in the chamber are adjusted until the laser beam reflects perfectly back on itself. A schematic representation of aligning the center of the sample with the ABB Extrel can be seen in Figure 4a. The purpose of aligning the incident and reflected beam is to assure the sample is perfectly aligned with the mass spectrometer (MS). Alignment with the MS allows for maximum signal to be obtained. Using the X and Y controls, the laser is then aligned with the center of the sample, seen in Figure 4b. This is to ensure the molecular beam will only interact with the sample, and not the copper sample mount or edges of the SAM. At the edges of the SAM there are defects that do not occur throughout the SAM, and would produce results that were not representative of the gas-surface interface. The next step in the alignment process is to rotate the sample mount exactly 30°, as indicated by the micrometer on the manipulator arm. The purpose of rotation is to ensure only gas scattering at a specular angle are monitored, this is seen in Figure 4c. Finally, the Y position is adjusted to reflect the laser directly through the source aperture, as seen in Figure 4d. Alignment of the laser with the source aperture assures that the molecular beam will hit the center of the sample, and a portion of the molecular beam will deflect into the mass spectrometer.

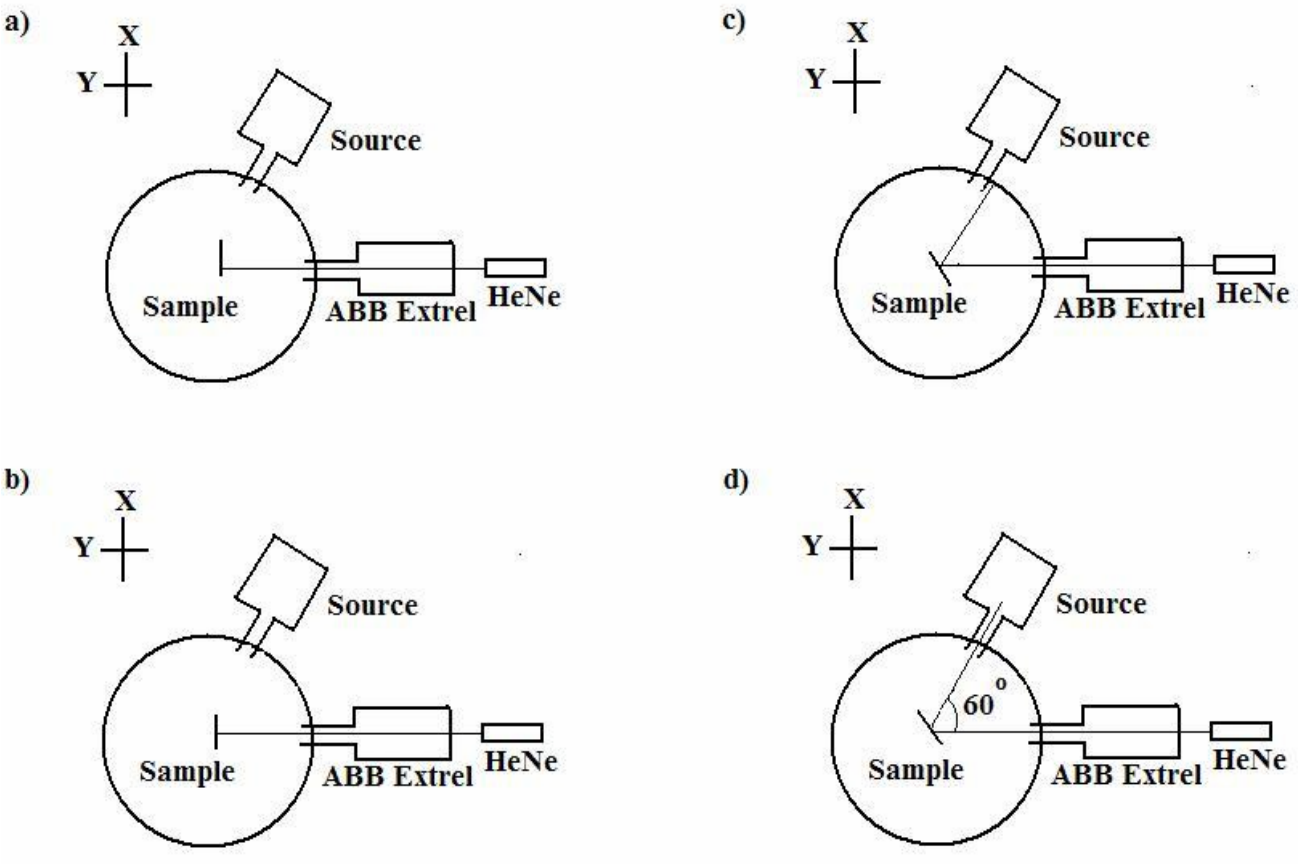

Figure 5. Schematic of the laser alignment process. a) The HeNe laser is aligned to reflect back on itself to ensure perfect alignment. b) The sample is adjusted in the X position to center the sample. c) The sample is rotated 30°, but the Y direction is not properly aligned. d) The Y position is adjusted such that the HeNe beam reflects directly into the source aperture.

When the sample has been properly aligned, the molecular beam is introduced into the chamber by opening a gate valve located between the main chamber and the third differential pumping stage in the source chamber. The gas molecules collide with the surface, and a small fraction of the gas molecules scatter at a final angle of 30°, into the MS. Once the gas molecules go through a colliminating aperture into the first differential pumping stage of the ABB Extrel, where the ionizer is located, a small percent of the gas molecules are pumped away while the majority proceeds into the ionizer, through focusing lenses, through a second aperture into the quadrapole rods, and then into the detector.

The TOF distributions of the scattered molecules are determined by monitoring the signal of the singly ionized parent mass peak of the molecule being scattered over the course of time.

The TOF scans are initiated when one of the slits on the chopper wheel passes a photogate, and a voltage pulse is sent to a multi-channel scaler.

The shapes and intensities of the TOF distribution were found to be highly reproducible, which allowed for comparison of several different gas-surface interfaces. All experiments presented here were done over the course of one day at a temperature of 298K. Conducting the experiments over the course of a single day minimize the effect of ambient changes, molecular beam intensity changes, or mass spectrometer changes.

2.6 Data Analysis

2.6.1 Raw Data

There are several timing corrections that need to be applied to the raw TOF data, to accurately determine the final energy distributions. The first timing correction accounts for the triggering pulse of the light emitting diode (LED) photogate. The time it takes the electrical signal to travel from the photogate to the computer is the electrical timing offset or t_{EO}. When one of the slits from the chopper wheel passes the photogate, the mass spectrometer software begins collecting TOF data. This happens despite the fact that the slit of the chopper wheel has not been reached, or has already reached (depending on the rotation direction of the chopper wheel) the source aperture, where the molecular beam enters the second differential pumping stage. The slits in the chopper wheel allow the molecular beam to proceed farther into the second differential pumping stage. When the chopper wheel is rotating in a counter-clockwise direction, the photodiode will be triggered prior to the molecular beam being let through the chopper wheel. When the chopper wheel is rotating in a clockwise direction, the molecular beam is allowed through the chopper wheel prior to the photodiode trigger pulse being initiated. The time differences between the trigger pulse and the beam entering the chamber leads to a second timing off set, the front-back offset or t_{FBO}. A schematic of the front-back offset is shown in Figure 5.

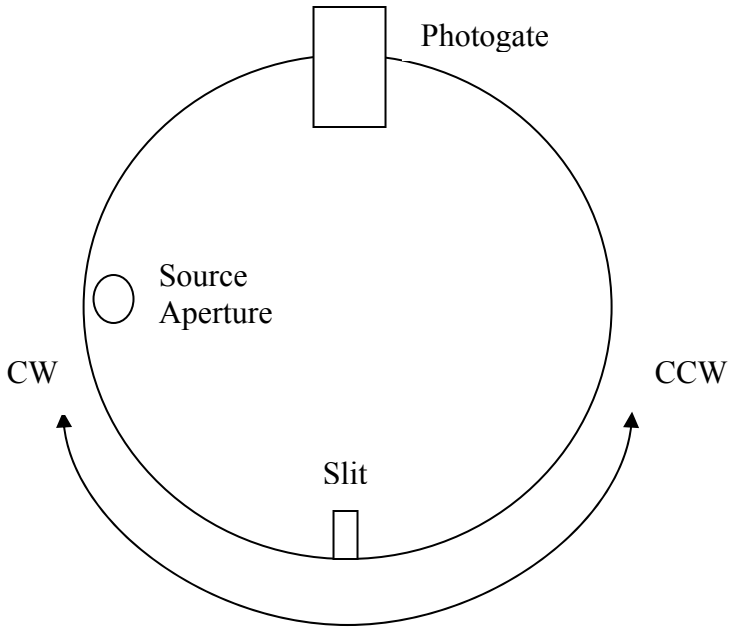

Figure 6. Once the slit reaches the photogate the chopper wheel must travel 90° before reaching the source aperture, allowing the beam to proceed on to the next differential pumping stage.

To determine the front-back offset, the chopper wheel is spun one direction and TOF data is collected. The chopper wheel is then spun the opposite direction and TOF data is again collected. The average of the difference in arrival times of the TOF peaks is the front-back timing offset. An additional measurement is made to measure the front-back offset.

The distance between peak pulses is measured using an oscilloscope, and these data were used to determine the frequency that the chopper wheel is rotating at in both clockwise and counter-clockwise directions. In this study the chopper wheel was spun in a counter-clockwise direction and had a single slit. Since there is one slit in the chopper wheel, the difference in peak arrival time is equal to the timing difference between the counter-clockwise and clockwise directions. Taking the time for half a revolution accounts for a single trigger pulse, which can be calculated from the data provided by the oscilloscope. For the chopper wheel spinning counter-clockwise at 250Hz the t_{FBO} was found to be 933μs.

The third and final timing offset accounts for the flight time of ions in the mass spectrometer. The mass spectrometer offset for the ABB Extrel was determined by B. Scott Day using a beam of carbon dioxide and xenon. The mass spectrometer offset is a constant

multiplied by the square root of the mass of the parent ion, $\alpha\sqrt{m}$. Day looked at several m/z ratios for both the carbon dioxide and xenon molecular beams, and created a calibration curve for the MS. From this calibration curve the constant, α, needed to determine the mass spectrometer timing offset, t_{MSO}, is 6.5, giving a MS offset of $6.5\sqrt{m}$ for a given species.

The equation used to calculate the true arrival time of the peak is:

$$t_{arrival} = t_{peak} - t_{FBO} - t_{EO} - t_{MSO}$$

The peak arrival time is obtained from the raw data. After all the timing corrections have been determined, they are subtracted from the raw data to provide the true arrival time of the peak. The true arrival time of the peak indicates how much time the gas spent on the surface sample, and the flight time from the surface to the mass spectrometer. The surface residence time of all the molecules studied in this investigation is expected to be less than 1 ns, which is several orders of magnitude lower than the sensitivity of the measurements made. Therefore, the final TOF distribution can be attributed to the energy transfer dynamics during the gas-surface collisions.

2.6.2 Time-of-Flight to Probability Distributions

The raw TOF number distribution data, N(t), is used to calculate the translational energy probability distribution, $P(E_f)$, of the gas atoms leaving the surface. The translational energy probability distributions are calculated based on final energy and the raw TOF number distribution, E_f and N(t). The relationships of E_f and N(t) are $E_f = 0.5m(d/t)^2$ and $P(E_f) \ \alpha \ t^2 \ N(t)$, where m is the mass of the gas, d is the flight distance from the surface to the mass spectrometer, and t is flight time.[9]

Using the relationships of N(t) and $P(E_f)$, translational energy probability distributions can be constructed by plotting $P(E_f)$ versus E_f. There are two main components of the translational energy distributions: the impulsive scattering (IS) and thermal desorption (TD). The TD component follows a Boltzmann distribution of the form $P_{TD}(E_f) = E_f(RT)^{-2} \exp(-E_f/RT_{surf})$.[9] The IS component of the translational energy probability distribution is the difference between the final translational energy probability distribution, $P(E_f)$ and the TD probability distribution, $P_{TD}(E_f)$.[9]

The two channels, IS and TD, investigated in this work have different characteristics. Impulsive scattering is characterized by gas atoms that promptly recoil from the surface,

transferring little to no energy to the surface. The thermal desorption component is due to gas atoms that recoil from the surface after thermalizing on the surface. Analysis of the IS and TD fractions provide information about the rigidity of the surface, gas-surface interactions, amount of energy the surface can dissipate, as well as any chemical process that may occur on the surface, such as proton exchange.

Chapter 3

Results and Discussion

3.1 Introduction

The properties of both the surface and the gas affect the energy transfer dynamics during the gas-surface collision. While there has been extensive research in the field of gas-surface dynamics, there have not been a large number of experiments conducted in the area of gas-surface dynamics of hydrogen bonding species. Nathanson and co-workers parallel our interests in this area.[9, 26-31]

Nathanson et al. have conducted a variety of studies that deal with scattering a number of gases from various surfaces.[9, 10, 27, 28, 32-34] In one such study, Ne, CH_4, NH_3, and D_2O were scattered from thin organic liquid films of squalane and glycerol. A schematic of these systems is shown in Figure 7. Nathanson et al. found that Ne and CH_4 thermally accommodated more efficiently on squalane than on glycerol. Opposingly, D_2O was thermally accommodated on glycerol much more extensively than on the squalane surface. NH_3, however, was thermally accommodated on both squalane and glycerol equally. From these observations, Nathanson and co-workers concluded that solubility trends loosely track gas-liquid energy exchange trends, but the scattering dynamics are not fully accounted for based on solubility trends alone. Based on the results of Nathanson et al., mechanical softness, chain length, and packing density of surface species, as well as overall surface roughness, structure, and defects must also play a role in gas-surface energy transfer dynamics.[9, 14, 27, 32-37] Additionally, the potential energy surface well-depth defining the gas-surface interactions must contribute to the energy transfer dynamics.

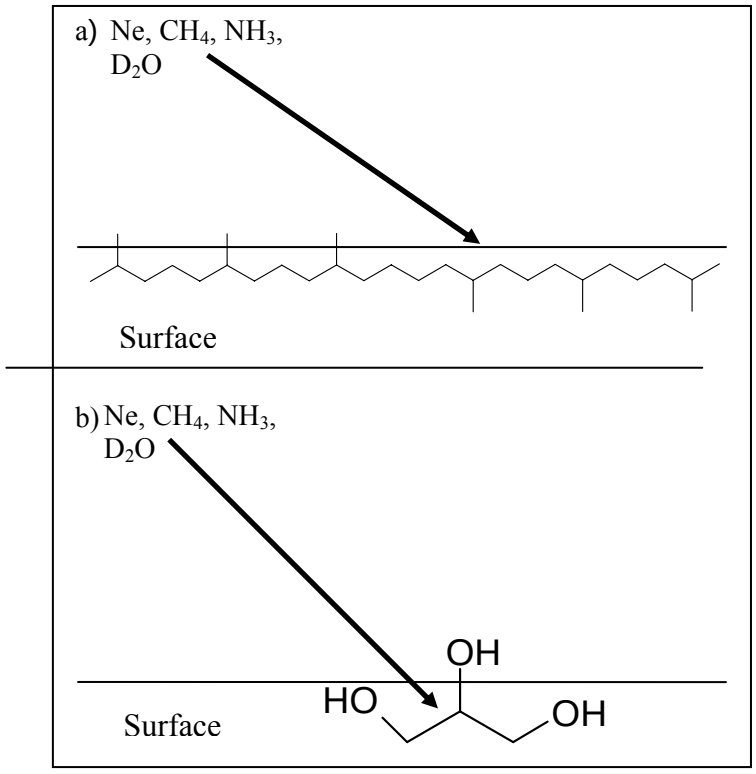

Figure 7. Gas-surface systems used in the Nathanson investigation into effect of hydrogen bonding.

The focus of our work is to further the understanding of the gas-surface energy transfer dynamics in polar and non-polar gas and surface species. We have investigated high energy Ne, CD_4, ND_3, and D_2O gases scattering from three alkanethiol derived surfaces with varying interfacial functionality. The three alkanethiol derived surfaces used in this study were $CH_3(CH_2)_{15}SH$, $NH_2(CH_2)_{11}SH$, and $OH(CH_2)_{16}SH$.

The purpose of this study is to develop a fundamental understanding of energy transfer dynamics in gas-surface collisions, explore how surface structure and functionality effect energy transfer and accommodation on the surface, and, finally, to determine how gas polarity effects energy transfer and accommodation.

3.2 Experimental

Approximately 2 % Ne, CD_4, ND_3, and D_2O, were seeded in 98 % H_2, or He to obtain hypothermal molecular beam energies. For Ne, CD_4, and ND_3, the desired amount of the pure gas was introduced into a mixing cylinder, using a gas regulator. The carrier gas, H_2, or He, was

introduced into the mixing cylinder in the same manner as the pure gas. After the gas is allowed to mix, and the lines that carry the gas mixture to the UHV chamber are purged, the beam energy is determined using the SRS residual gas analyzer.

To make a seeded beam of D_2O, a small amount of D_2O was placed in the bottom of a glass bubbler that had been thoroughly cleaned and rinsed with D_2O. The bubbler was then submerged in a digitally temperature-controlled water bath. By varying the temperature, the beam energy was tuned. Once submerged into the water bath, the carrier gas was passed through the bubbler. The lines carrying the D_2O were purged, and the beam was introduced into the UHV system. The beam energy was characterized in the same manner as the other molecular beams (see section 2.4 for a complete description).

The raw TOF data was used to calculate the translational energy probability distribution, $P(E_f)$, of the gas atoms leaving the surface based on the translational energy distribution being proportional to flight time, t, and number density, N(t). The translational energy distributions were calculated from the following relationships for E_f and N(t): $E_f = 0.5m(d/t)^2$ and $P(E_f) \sim t^2 N(t)$. In these equations, m is the mass of the gas, d is the flight distance from the surface to the mass spectrometer, and t is flight time as described in section 2.6.2.[9] There are two main channels of interaction between the impinging gas molecule and the surface that were examined during the scattering experiments. These two channels are the impulsive scattering channel and the thermal desorption channel.

Impulsive scattering (IS) is due to gas atoms that recoil from the surface and transfer little energy to the surface, likely having only a single, or a few collisions with the surface. The thermal desorption (TD) component is due to gas atoms that recoil off the surface after thermalizing on the surface. The extent of IS and TD fractions in scattering provide information about how energy transfer dynamics depend on the rigidity of the surface, the gas-surface interaction, the amount of energy the gas can dissipate throughout the surface, as well as any chemical process that may occur on the surface.

3.3 Characterization of SAMs

To assess how well ordered the SAM was, reflection-absorption infrared spectroscopy (RAIRS) was used. Panel a, of Figure 8, shows the RAIR spectrum for the methyl terminated SAM with a CH_2 asymmetric stretch at 2918 cm^{-1}. A CH_2 asymmetric stretch at 2918 cm^{-1} is

indicative of a well-ordered, crystalline-like structure with few defects. The asymmetric methylene stretch may be red shifted for extremely well ordered films.[38, 39] Panel b, of Figure 8, shows the RAIR spectrum for the hydroxyl terminated SAM with a CH_2 asymmetric stretch at 2917 cm^{-1}, indicating a well-ordered monolayer. One would expect to see a hydroxyl stretch between 3100-3600 cm^{-1} with traditional FTIR spectra, but with RAIRS this hydroxyl stretch is not seen due to surface selection rules, as well as broadening of the hydrogen bond peaks.[40] Shown in panel c, of Figure 8, is the RAIR spectrum of the amine terminated SAM, with a CH_2 asymmetric stretch at 2924cm^{-1}, this indicates a less ordered structure that is due in part to the fewer methylene units present in the chain, and the presence of the bulky charged species prior to the TEA rinse. Fewer methylene units in the amine terminated SAM leads to fewer chain-chain interactions. Reduced chain-chain interactions produce a less ordered system.[39]

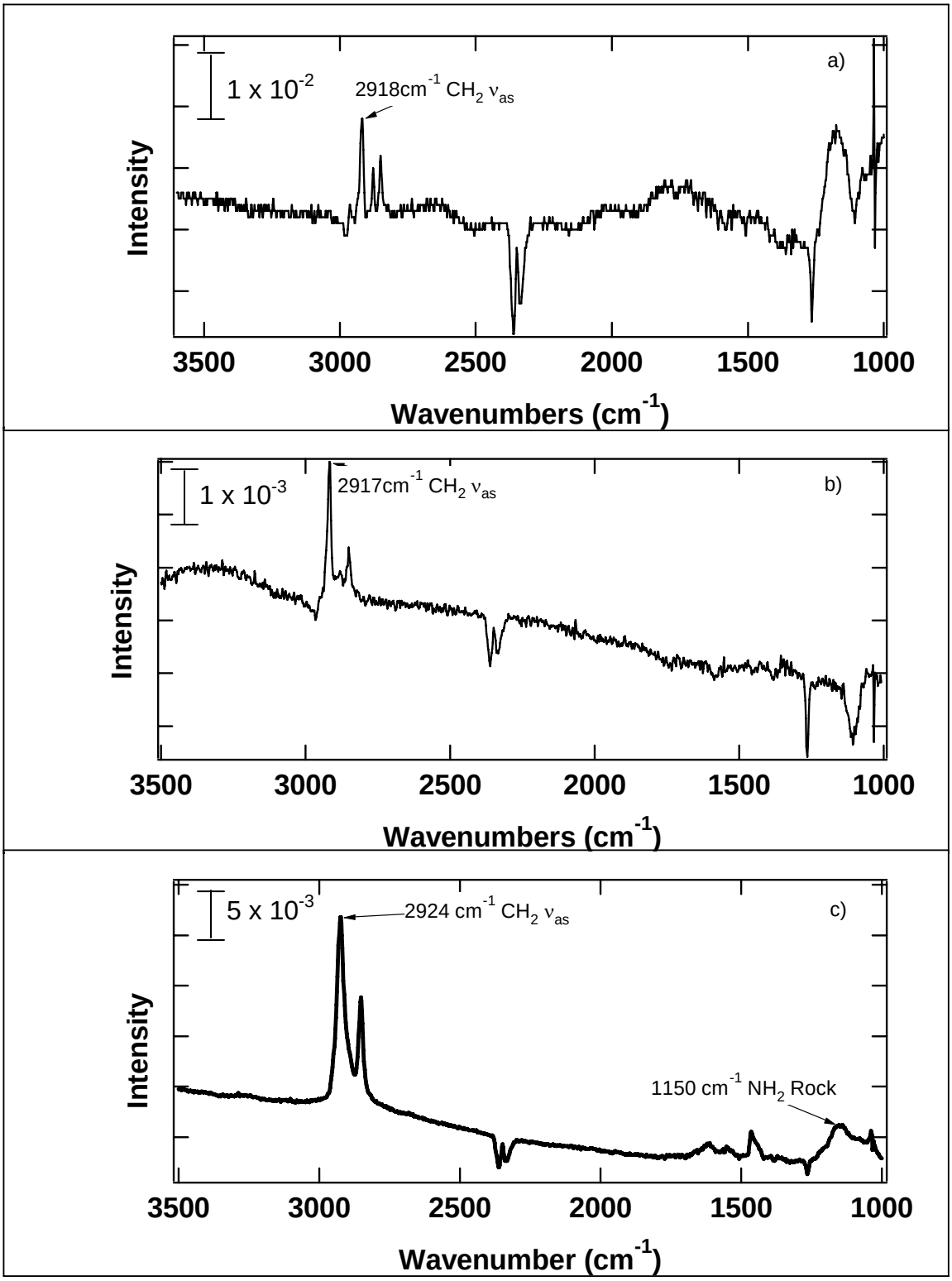

Figure 8. RAIR spectra of the surfaces used in this study, at room temperature. a) RAIR spectrum of $HS(CH_2)_{15}CH_3$ surface b)RAIR spectrum of the $HS(CH_2)_{16}OH$ c) RAIR spectrum of the $HS(CH_2)_{11}NH_2$ surface

A second surface characterization technique, X-ray photoelectron spectroscopy (XPS), was used to characterize the amine terminated SAM. XPS was used to confirm that the TEA rinse removed the chloride ion from the surface. The chloride 2s region of the XPS spectrum is shown in Figure 9. The absence of a peak at 274 eV indicates that there is no chloride ion present on the monolayer, within the sensitivity of the instrument.

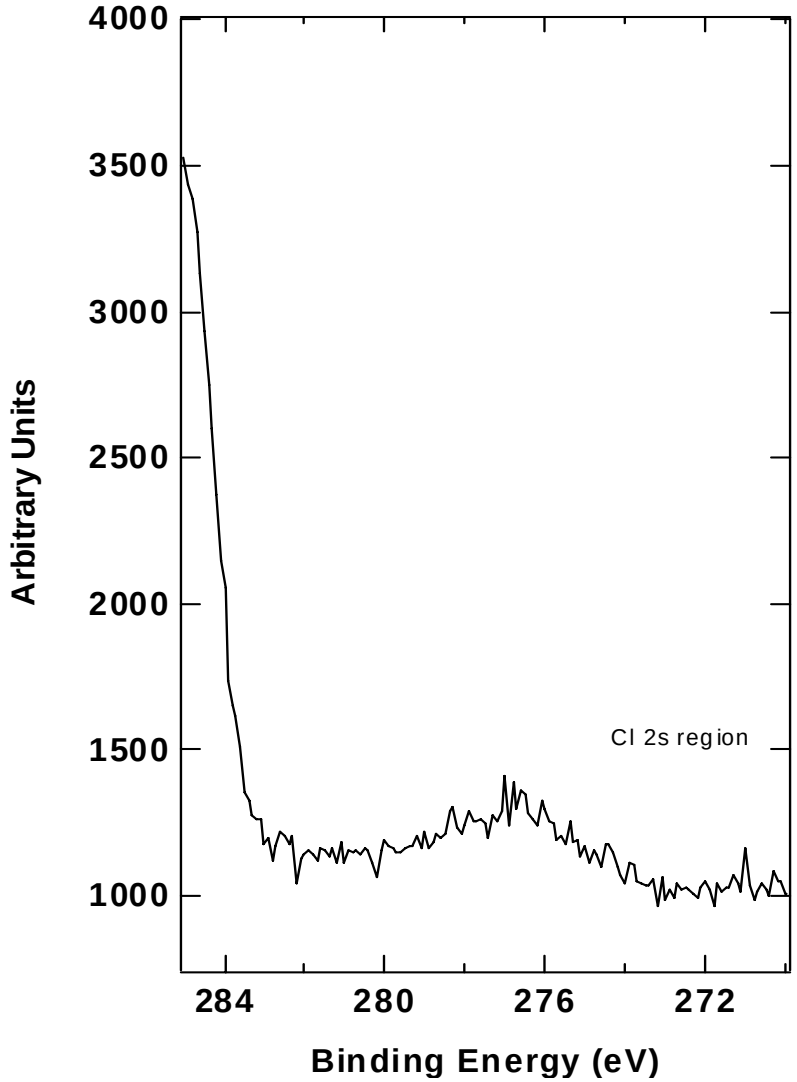

Figure 9. XPS spectra of the amine terminated surface after being rinsed with TEA.

3.4 Time of Flight Data

3.4.1 Time of Flight Data Summary

Figures 10 and 11 show the TOF data and Table 2 summarizes the IS and TD fractions for Ne, CD_4, ND_3, D_2O gases scattering from the methyl, amine, and hydroxyl terminated surfaces. Ne tends to thermally accommodate on the surfaces in the order of CH_3 > OH > NH_2, as shown in Table 2. The order of thermal accommodation corresponds to the mechanical softness of the SAM; therefore the CH_3 terminated surface is the softest, while the NH_2 and OH terminated surfaces are the more rigid. This assessment of mechanical softness of the surface can be made because Ne is inert, and will have very little attraction, or interaction, with the surfaces. Likewise, CD_4 is significantly more thermally accommodated on the CH_3 terminated surface than on the polar surfaces. The greater accommodation reflects the mechanical properties of the CH_3 terminated surface, and the greater attraction of the CD_4 to the CH_3 terminal groups, as one would predict based on the solubility trends in Table 1. The ND_3 thermally accommodates almost equally on both the polar and non-polar terminated surfaces. Based on the solubility data reported in Table 1, one would not predict ND_3 to thermally accommodate equally well on all surfaces. Finally, the D_2O scattering shows that the strongest hydrogen bonding gas has the greatest thermal accommodation on the strongest hydrogen bonding surface. One would predict this behavior of D_2O scattering based on the solubility trends reported in Table 1.

3.4.2 Impulsive Scattering and Trapping

The impulsive channel of the TOF spectrum is indicative of the portion of molecules that do not transfer enough energy, upon collision, to become accommodated on the surface. The impulsive scattering (IS) channel can be illustrated by two spheres inelastically colliding with one another. When the inelastic collision between the sphere representing the gas and the sphere representing the surface occurs, some portion of the gas's energy is transferred to the surface. If there is a greater attractive force between the sphere representing the gas and the sphere that represents the interfacial functional group, then energy transfer from the gas to the surface will be enhanced. An impinging molecule can also experience multiple collisions, transfer much of its energy to the surface, and then desorb into the gas phase. This is the trapping-desorption (TD). Once a gas molecule becomes thermally equilibrated on the surface, one of three events

can occur within the TD channel. First, the trapped molecule can enter the surface, undergo a chemical reaction, and then desorb back into the gas phase. A second possibility is that the trapped molecule can enter the monolayer, react or not react, and then desorb into the gas phase. The third possibility is that the trapped molecule can become thermally accommodated on the surface, and then simply evaporate back into the gas phase. All three of these components make up the TD channel. For the gas-surface systems explored here, we expect to observe primarily non-reactive scattering events. The only possible reaction for these systems to undergo is proton exchange between the D_2O and ND_3 gases with the NH_2 and OH terminated SAMs. The data indicates that proton exchange does not occur in these systems.

The TOF spectra are composed of both IS and TD channels. Analysis of these two channels allows insight into the gas-surface forces (i.e. dipole-dipole and hydrogen bonding effects), as well as providing awareness of the microscopic mechanisms of the gas-surface collisions, and evaluation of the importance of potential energy surface well depths characteristics in the outcome of a gas-surface collision.

3.4.3 Data

Figures 10 and 11 show the raw and processed TOF data for the 60 kJ/mol Ne scattering from the CH_3 terminated SAM, OH terminated SAM, and the NH_2 terminated SAM, respectively. The raw and processed data for the scattering of polyatomic gases are shown in Figures 12 a-c and 13 a-c. The raw data, number distribution, N(t), and spectra are a plot of the detector signal at m/z = 20 versus flight time for the molecules to traverse the distance between the surface and the mass spectrometer ionizer. The raw signal, seen in Figures 10 and 12, is proportional to the number density, N(t). N(t) is used to calculate the probability of final energy distribution, $P(E_f)$. $P(E_f)$ distribution is the probability that a Ne molecule will leave the surface with a final energy of E_f. The $P(E_f)$ distributions are shown in Figures 11 and 13, and are calculated using the equation $E_f = 0.5m_{Ne}(L/t)^2$ and $P(E_f) \alpha t^2N(t)$. The final energy distribution seen in Figures 11 and 13 are separated into the impulsive scattering (IS) and thermal desorption (TD) components. The TD component is the low energy portion of the spectrum that falls within a Boltzmann distribution of functional form $P_{TD}(E_f) = E_f(RT)^{-2}\exp(-E_f/RT_s)$. The Boltzmann distributions are represented in Figures 10, 11, 12 and 13, and are represented by the solid curve.

The IS component of the energy distribution is determined by the difference between $P(E_f)$ and $P_{TD}(E_f)$.

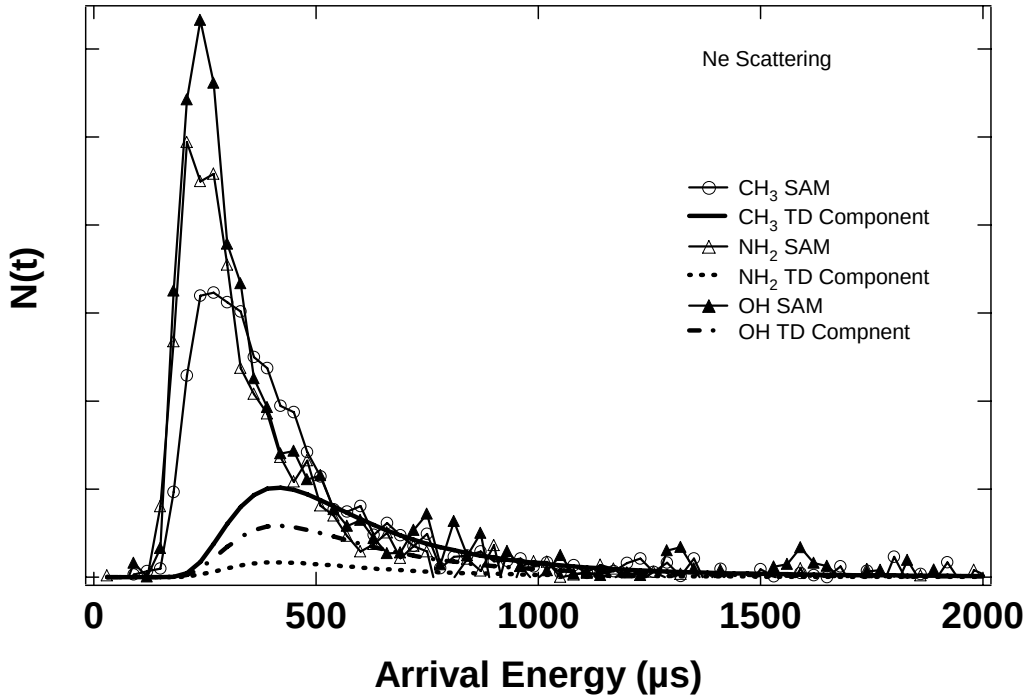

Figure 10. TOF Spectra for 60 kJ/mol Ne scattering from $HS(CH_2)_{15}CH_3$, $HS(CH_2)_{16}OH$, and $HS(CH_2)_{11}NH_2$ SAMs on Au at a surface temperature of 295K.

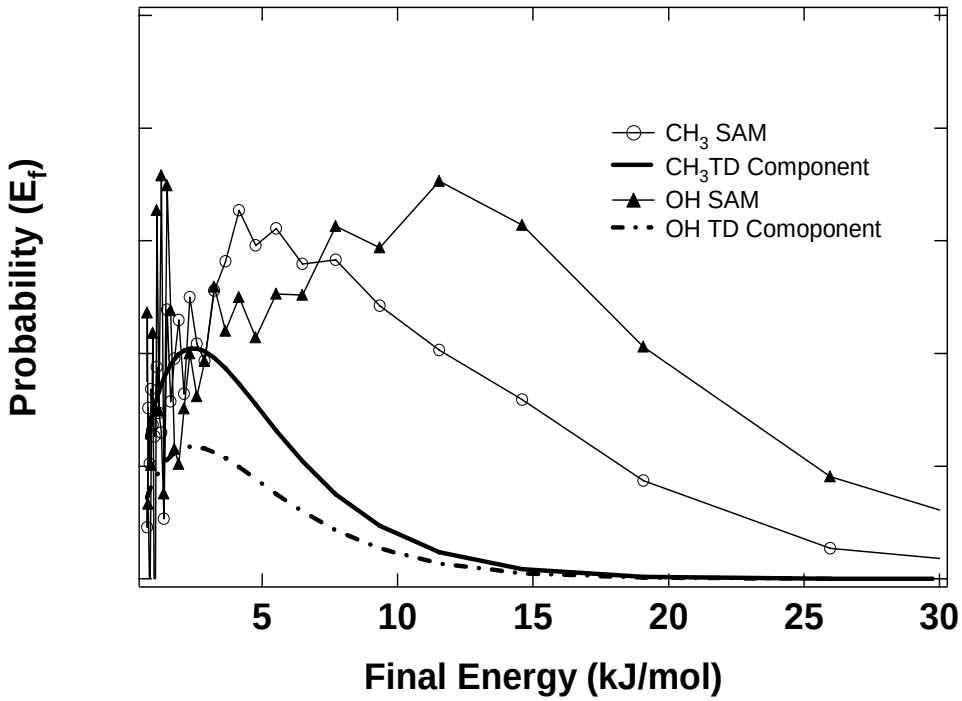

Figure 11. Final energy distributions for Ne scattering from $HS(CH_2)_{15}CH_3$, $HS(CH_2)_{16}OH$, and $HS(CH_2)_{11}NH_2$ SAMs on Au at a surface temperature of 295K.

Table 2 summarizes the percent of TD and IS components for all the systems examined in this study. From this table, it can be seen that thermal accommodation of Ne on the surface occurs in the order $CH_3 > OH \sim NH_2$. The decrease in the ability of the hydroxyl and amine terminated SAMs to thermally accommodate Ne on the surface is most likely due to the ability of the surface hydroxyl and surface amine groups to hydrogen bond to one another. This makes the surface appear more rigid to the impinging Ne gas. The hydrogen bonding of the hydroxyl and amine terminals quenches the low energy, high amplitude surface motions, such as wagging, that have been shown to promote efficient energy transfer.[41] Less efficient energy transfer leads to a greater IS channel. The surface with the methyl terminated group allows for these surface motions to be initiated when Ne impinges on the surface, thus Ne transfers more energy to the surface. Due to the inert, monatomic nature of Ne, it cannot transfer energy to internal modes of rotation and vibration when it collides with the surface, and therefore can be used as an estimate of mechanical roughness and softness of the SAM. By comparison of Ne scattering with scattering of polyatomic gases, it may be possible to estimate the intermolecular interactions between the gases and surface that are responsible for the increased fraction of thermal accommodation.

Several trends can be seen in Table 2 when examining the scattering dynamics of the polyatomic gases. The first trend that is noticed is that CD_4, a non-polar gas, not capable of hydrogen bonding, is most extensively thermally accommodated on the non-polar SAMs. CD_4 experiences a similar extent of thermal accommodation on the NH_2 and OH terminated surfaces. The extent of thermal accommodation of CD_4 on all the surfaces are shown in Figure 12 in panel a. The increasing Boltzmann component as one proceeds from the OH to the NH_2 to the CH_3 terminated SAM indicates more thermal accommodation. The second trend that can be seen from Table 2, with regards to the scattering of polyatomic gases, is that the polar gases that are capable of hydrogen bonding (ND_3 and D_2O) thermally accommodate only slightly better on polar surfaces (NH_2 and OH). In the case of ND_3, the increase in the extent of thermal accommodation indicates that there exists some attractive force between the gas and the surface, due to the fact that ND_3 accommodates almost equally on all the surfaces despite the presence of a wide range of physical and chemical properties of the surfaces. This is indicated by Table 2, Figure 12 panel b, and Figure 13 panel b. One would expect that if surface rigidity alone controlled scattering dynamics, ND_3 would thermally accommodate in the same manner as Ne. An interesting feature of Table 2, Figure 12 panel c, and Figure 13 panel c, is that D_2O thermally accommodates in the order of $CH_3 < NH_2 < OH$. This significant increase, 10%, in the extent of thermal accommodation is most likely due to the increased interactions (hydrogen bonding) between the protic, polar D_2O and the protic, polar OH interfacial functional group. From Figures 11, 13, and Table 2 the overall trend for thermal accommodation on the CH_3 surface is $Ne < CD_4 \approx ND_3 \approx D_2O$. The trend for both the NH_2 and OH surface is $Ne < CD_4 < ND_3 < D_2O$. When the IS and TD fractions from Table 2 are compared, it is evident that the polar surfaces are more sensitive to the composition of the gas that is being scattered than are the non-polar surfaces, as demonstrated by the larger range in IS and TD fractions for the NH_2 and OH terminated surfaces.

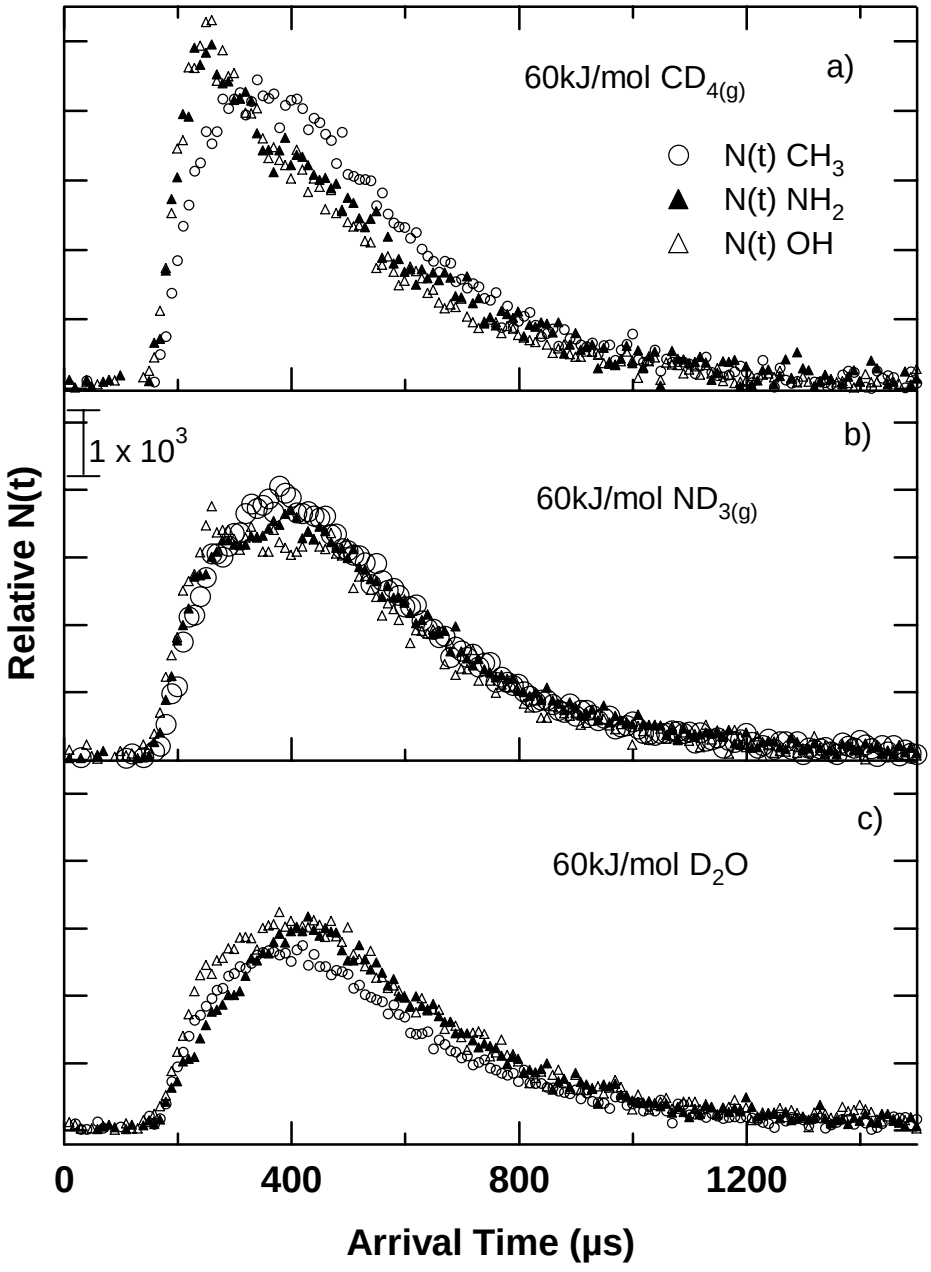

Figure 12. a) TOF spectra, N(t), for 60 kJ/mol CD_4 scattering b) TOF spectra, N(t), for 60 kJ/mol ND_3 scattering c) TOF spectra, N(t), for 60 kJ/mol D_2O scattering. The gases were scattered from $HS(CH_2)_{15}CH_3$, a $HS(CH_2)_{16}OH$, and a $HS(CH_2)_{11}NH_2$ SAMs on Au at a surface temperature of 295K.

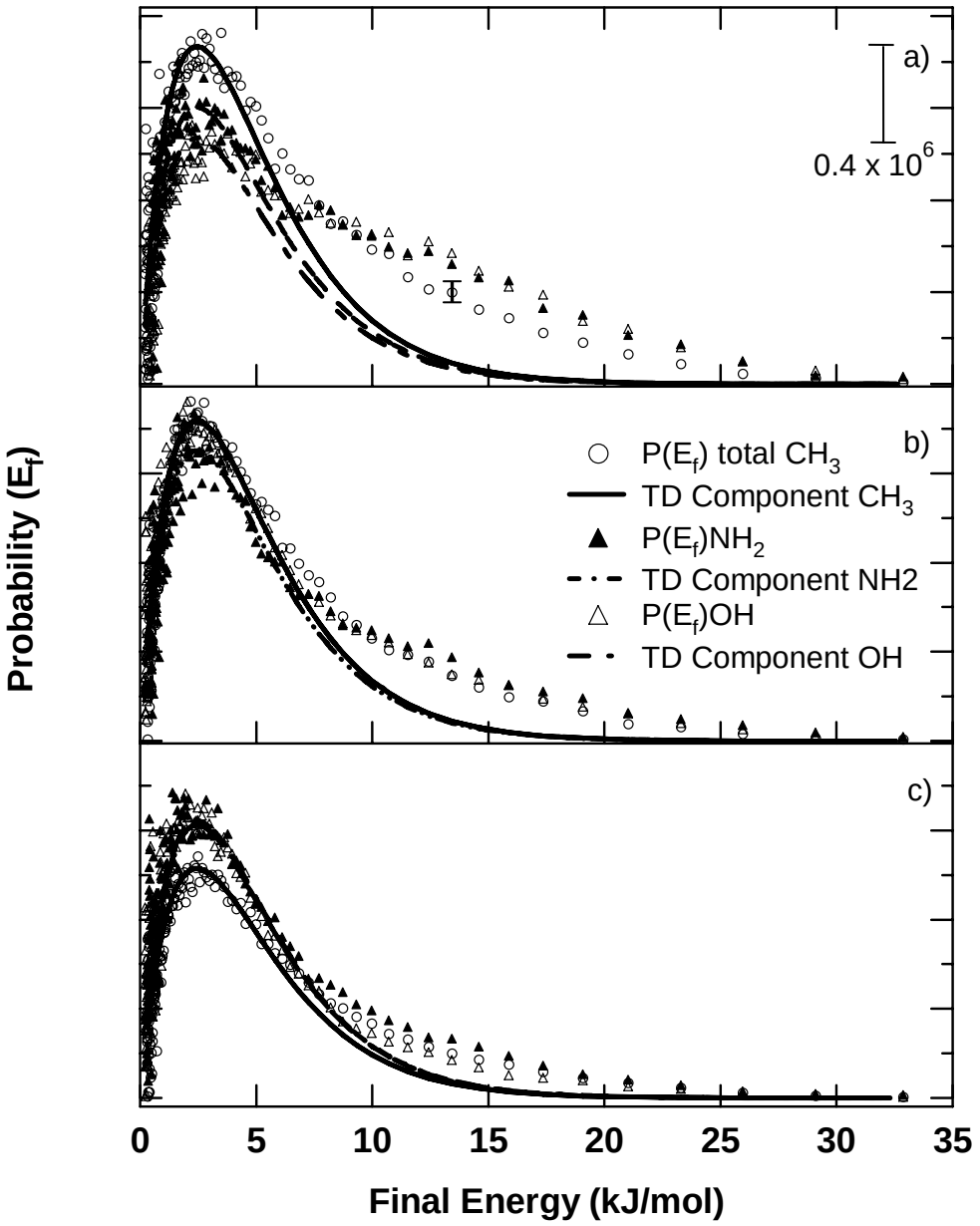

Figure 13. Final energy distributions of a) 60 kJ/mol CD_4 scattering b) 60 kJ/mol ND_3 scattering c) 60 kJ/mol D_2O scattering. All gases were scattered from $HS(CH_2)_{15}CH_3$, $HS(CH_2)_{16}OH$, $HS(CH_2)_{11}NH_2$ SAMs on Au at a surface temperature of 295K.

Table 2. Summary of the IS and TD fractions.

	Ne (60 kJmol^{-1})		CD_4 (60 kJmol^{-1})		ND_3 (60 kJmol^{-1})		D_2O (60 kJmol^{-1})	
Surface	IS (%)	TD (%)	IS (%)	TD (%)	IS (%)	TD (%)	IS (%)	TD (%)
CH_3	61	39±3 %	30	70±1 %	22	78±1 %	21	79±1 %
NH_2	77	23±3 %	41	59±1 %	28	72±1 %	20	80±1 %
OH	88	22±3 %	47	53±1 %	22	78±1 %	11	89±1 %

3.5 Discussion

Insight has been gained into the energy transfer dynamics at the gas-surface interface of potentially hydrogen bonding species. Gaseous Ne, CD_4, ND_3, and D_2O have been scattered from surfaces terminated with CH_3, NH_2, and OH functional groups. Ne scattering has allowed for the assessment of mechanical roughness of the surfaces. It was found that the CH_3 terminated surface was approximately 16 % to 27 % softer than the hydrogen bonding terminated surfaces of NH_2 and OH. Based on this result, one would predict that if mechanical roughness alone controls the energy transfer dynamics at the gas-surface interface, then all the scattered gases would thermally accommodate best on the CH_3 terminated surface. However, we find that ND_3 and D_2O have an increased extent of thermal accommodation on the NH_2 and OH terminated surfaces. This result leads to the conclusion that there is some attractive force between gases and surfaces that are capable of hydrogen bonding. The attractive force (or forces) responsible for the increased extent of thermal accommodation could be due to the increased internal degrees of freedom for the polyatomic gases and potential energy surface well depths. These two possibilities and surface rigidity are explored in the following sections.

3.5.1 Surface Rigidity

Atomic roughness of a surface has been shown to significantly affect energy transfer dynamics.[32, 37, 42, 43] If atomic roughness effects energy transfer dynamics, then the packing density, order, and rigidity of the surface should also effect energy transfer dynamics. It has been shown that methyl and hydroxyl terminated SAMs have similar packing densities.[24, 38, 44] Through the use of RAIRS we have shown that both the methyl and hydroxyl terminated SAMs are well-ordered, as indicated by the methylene unit asymmetric stretch below 2918 cm^{-1}. If both the methyl and hydroxyl terminated surfaces have similar packing and ordering structures, then it is reasonable to conclude that the surfaces must differ in rigidity, based on the Ne scattering data. If both surfaces had equal packing density, order, and surface roughness, one would expect the extent of thermal accommodation to be nearly the same on both surfaces when Ne is scattered, however experimentally this is not the case. Far greater thermal accommodation of Ne is seen on the methyl terminated SAM, therefore it can be concluded that the methyl terminated surface is softer than the hydroxyl terminated SAM. It is believed that the increased rigidity of the hydroxyl terminated SAM is due to a hydrogen bond. This argument can be applied to the amine terminated SAM as well.

3.5.2 Internal Degrees of Freedom

Nesbitt and co-workers have recently reported that when CO_2 collides with the liquid surface of glycerol, squalane, or PFPE, energy is transferred readily from the surface to rotational modes of CO_2.[45] If the work of Nesbitt et al. is extrapolated to our study, then one may predict that Ne scattering would produce the smallest extent of thermal accommodation on the surfaces, because Ne is incapable of transferring energy from the surface to higher rotational modes. Ne cannot transfer energy to higher rotational modes because higher rotational modes do not exist within Ne. It may be possible to correlate heat capacity to internal degrees of freedom for the gas-surface interface.

As specific heat capacity increases there is an increase in the internal degrees of freedom. The specific heat capacity of the hydrogen analogs of the gases used in this study can be seen in Table 3. Based on specific heat capacity scaling with internal degrees of freedom, one would expect the order of thermal accommodation of the gases on each surface to be $Ne < CD_4 < ND_3 < D_2O$. However, this order of thermal accommodation is not followed for the

hydrogen bonding surfaces. Therefore, there must be an additional factor that contributes to how thermal accommodation occurs at the gas-surface interface, such as potential energy surface well-depth.

Table 3. The specific heat capacities at constant volume of the hydrogenated gases examined in this study.

Gas Species	Specific Heat Capacity (kJ/mol K)
Ne	0.012
CH_4	0.027
NH_3	0.028
D_2O	0.034

3.5.3 Potential Energy Surface Well-Depth

3.5.3.1 Experimental Potential Energy Well-Depth and Prediction of Energy Transfer Dynamics

Nathanson and co-workers have established a correlation between the solvation enthalpies measured from the temperature dependence of Henry's Law equilibrium constants, $K_H = \chi_{soln} / P_{gas}$, where χ is the solute mole fraction in solution, and P_{gas} is the solute gas pressure.[9, 46] ΔH^o_{solv} is used to estimate the Gibbs free energy, $\Delta G° = \Delta H° - T\Delta S$, of the solvated and gas species. Where $\Delta G°$ is the change in Gibbs free energy at the standard state, $\Delta H°$ is the change in enthalpy of solvation at the standard state, T is temperature of the surface, and ΔS is the change in entropy of the surface upon a gas-surface collision. It can be approximated that ΔS is negligible because when the gas- surface collision occurs, the surface is disrupted very little, and therefore should not change the Gibbs free energy significantly. If the change in entropy is small then enthalpy of solvation can be used to approximate Gibbs free energy. The enthalpy of solvation values for systems similar to ours are shown in Table 4. To compare the solvation enthalpies for a hydrogen bonding surface, methanol is used as a model for the hexadecanol.[47, 48] Enthalpy of solvation values are indicative of how attracted the two species are to one another; because of this, we use enthalpy of solvation and an indication of potential energy surface well-depth. As enthalpy of solvation increases, both the attractive force between the species and the potential energy surface well-depth increases.

Table 4. Enthalpy of solvation values for systems similar to the ones investigated in this study.

Systems	**$\Delta H°_{solv}$ (kJ/mol)**
Ne, decane	6.5
CH_4, decane	-4.3
NH_3, hexadecane	-6.9
H_2O, hexane	-17
Ne, methanol	5.7
CH_4, methanol	-3.7
NH_3, methanol	-12
H_2O, methanol	-47

Enthalpy of solvation data may allow for prediction of energy transfer dynamics at the gas-surface interface, because the chemical forces that drive solution phase chemistry may play a role in the degree a gas is attracted to a surface. Based on the strength of those chemical forces, the extent of thermal accommodation may be affected. Based upon solvation enthalpy data, one would predict that Ne and CD_4 would thermally accommodate almost equally on the aprotic and protic surfaces. Although Ne adheres to this prediction, CD_4 accommodates much more readily on the aprotic surface. For ND_3, one may expect better accommodation on the protic surfaces, however we observe ND_3 accommodating equally well on both protic and aprotic surfaces. Based on solvation enthalpies, one would expect D_2O to accommodate best on protic surfaces. We observe this behavior for the OH terminated surface. Further analysis of the scattering trends is presented in Figure 14. Figure 14 shows the solubility of the gases in bulk solutions that are representative of our interfacial functional groups. As the natural log of the Henry's law constant increases, the gases proceed from Ne, CD_4, ND_3, to D_2O for both the methyl and hydroxyl terminated SAMs. The trends seen in Figure 14 are similar to those seen in the solvation enthalpy data. From the solubility data, one would expect Ne and CH_4 to accommodate nearly equally on the hydroxyl terminated surface due to the proximity of the natural log values. However, Ne accommodates less readily as indicated by the large gap in the TD fraction value. One would expect large difference in TD fraction based on the range of the natural log of Henry's law constants. Experimentally, we observe approximately a 30 percent difference in TD fractions. For the methyl terminated surface, based on Henry's law solubility constants, one would expect the difference in thermal accommodation to be equal when Ne versus CD_4 is scattered and when CD_4 versus ND_3 or D_2O are scattered. This prediction is due to the equal value in spacing for Henry's law constants. However, experimentally, there is a

larger range in Ne versus CD_4 scattering then CD_4 versus ND_3 and D_2O scattering. Based on the experimental results, bulk properties alone, as an indication of potential energy surface well-depth, do not allow for quantitative predictions of the extent of thermal accommodation at the gas-surface interface, but do allow for qualitative prediction. After examining experimental potential energy surface well-depth, enthalpy of solvations, theoretical potential energy well depths were examined.

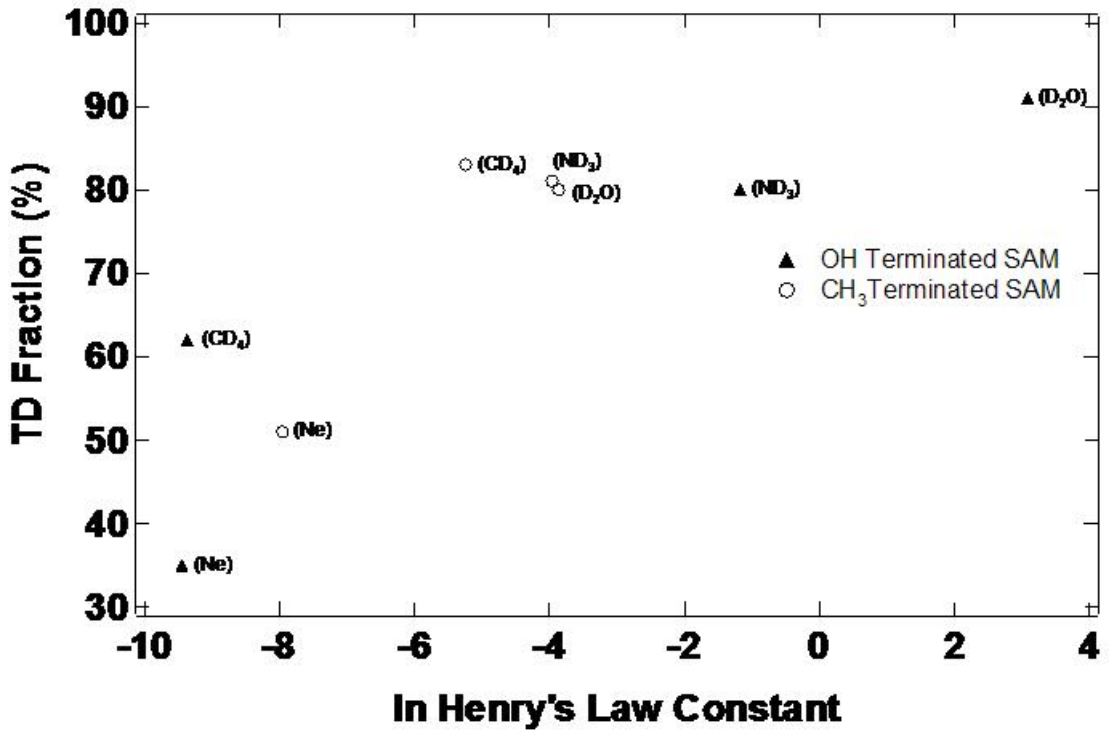

Figure 14. A plot of thermal accommodation fraction as a function of K_H.

3.5.3.2 Potential Energy Surface Well-Depth and the Prediction of Energy Transfer Dynamics

Ab initio calculations were carried out to model the well-depth of the gas-surface systems, discussed above, by Troya and co-workers. These calculations were performed so a deeper understanding of the gas-surface interactions might be gained. Through the use of *ab initio* calculations, one can begin to gain insight into how the relative well depths of the potential energy surfaces affect the energy transfer dynamics. The well depths were calculated based on

the gas molecule approaching a model of the surface terminal group. Ethane, methyl amine, and methanol were used as mimics for the ethyl termini of the methyl, amine, and hydroxyl terminated surfaces, respectively. The X-H bond, where X = O, N, or C, of the probe gas (Ne, H_2O, NH_3, or CH_4) approaches the Y-C bond, where Y = C, N, or O, of the surface mimic (CH_3CH_3, CH_3NH_2, or CH_3OH) in a collinear orientation. The X-Y distance was scanned from 5.0Å to 3.0Å with steps of 0.1Å. The area around the minima was scanned with a step of 0.01Å. All calculations were performed at the MP2/aug-cc-pvtz level using the counterpoise method to correct for basis set superposition error using Gaussian 03.[49] All of the calculations are based solely on hydrogen and not deuterium. The use of hydrogen and not deuterium in the calculations does not matter, due to the fact that the calculations are based upon electronic structure and not the core nucleus of the atom.[50]

Table 5 shows the locations and depths of the Van der Waals well minima between the gases Ne, CH_4, NH_3, and H_2O with CH_3CH_3, CH_3OH, and CH_3NH_2. From Table 5 it can be seen that the hydrogen bonding gases (NH_3 and H_2O) interact most strongly with the polar surface mimics (CH_3OH and CH_3NH_2), with the strongest interaction being between H_2O and methanol. Some correlation is seen between the Van der Walls well depths and the experimental results (i.e. TD fraction increases with increasing well-depth). However, as seen in Table 5, well depths for the ethane systems with the hydrogen bonding gases do not follow the trends seen in the experimental data. Based on Table 5, one would predict that the order of accommodation on the methyl surface would be $D_2O > ND_3 > CD_4 >$ Ne. Experimentally, however, it is noted that all the protonated gases accommodated almost equally on the methyl terminated surface. Based upon the experimental results, it is believed that the methyl terminated surface can act as an "inert", or baseline surface, to base the rest of the computational results off of. This is indicated by the ΔCH_3CH_3 well depths due to the methyl terminated surface thermally accommodating the polyatomic gases nearly equally, which have similar internal degrees of freedom. By subtracting the ethane system well depths from the other two surface mimics, the influence of increasing gas-surface interactions due to introduction of polar surface groups on the scattering dynamics can be better understood. This is demonstrated by the similar ΔCH_3CH_3 values of H_2O scattering from the amine surface mimic and NH_3 scattering from the hydroxyl surface mimic. If the well depths alone are examined for these two systems, it is clear that the depths are very different, and the similar behavior of the systems, based on the experiments, would not be seen.

The ΔCH_3CH_3 well-depth trends calculated from theory for the individual surface mimics match the trends of the experiments. For the amine and hydroxyl surface mimics, the energy transfer dynamics are $H_2O > NH_3 > CH_4 >$ Ne. Specifically, what can be gained from the theory is the hydrogen bonding and dipole effects. The ΔCH_3CH_3 well- depths for the CH_4 gas scattering from the polar mimics indicates the dipole effects at the gas-surface interface (Ne is not indicative of dipole/induced dipole effects at the gas-surface interface due to the lack of available orbitals). Comparing the ΔCH_3CH_3 well depths of the methylamine and methanol systems, the extent to which each surface is capable of experiencing dipole-induced dipole effects, and the extent of hydrogen bonding capability, is apparent. The ΔCH_3CH_3 well depths for the hydroxyl mimic are much larger than those of the amine mimic, thus indicating that the hydroxyl surface has more capability of hydrogen bonding.

Table 5. Calculated potential energy surface well depths, minimum approach distance, and the well depth referenced to the methyl surface mimic for methyl, amine, and hydroxyl surface mimics with gases scattered from the surfaces.

System	r_{min} (Å)	Depth (kJ/mol)	ΔCH_3CH_3 Depth (kJ/mol)
CH_3CH_3 Surface Mimic			
Ne	3.54	0.518	---
CH_4	4.08	1.798	---
NH_3	3.77	3.053	---
H_2O	3.51	4.627	---
CH_3NH_2 Surface Mimic			
Ne	3.49	0.462	-0.056
CH_4	3.94	1.983	0.185
NH_3	3.61	4.460	1.407
H_2O	3.29	8.436	3.809
CH_3OH Surface Mimic			
Ne	3.29	0.473	-0.045
CH_4	3.79	2.033	0.235
NH_3	3.37	6.674	3.621
H_2O	3.15	9.600	4.973

3.6 Summary

The goal of this research was to establish an understanding of how a gas-surface reaction is first initiated by studying the gas-surface energy transfer dynamics. Through use of an UHV environment, molecular beams, and SAMs, we have gained insight into how polar and non-polar gases thermally accommodate on hydrogen bonding and non-hydrogen bonding surfaces.

This research found that, despite the gases having very different chemical properties, methyl surfaces are indifferent to the investigated polyatomic scattering gases. It has also been

established that weak hydrogen bonding gases, such as ND_3, have similar scattering dynamics from both polar and non-polar surfaces. Experimentally, it has also been found that strong hydrogen bonding gases are most sensitive to the polarity of the organic surfaces.

There has been some success in correlating the potential energy surface well depths of the gas-surface systems with energy transfer dynamics. The use of heat of solvation as an indication of potential energy surface well-depth has allowed for loose correlation of potential energy surface well depths with how a gas will be thermally accommodated on the surface. The use of computational methods as a direct indication of potential energy surface well-depth has also allowed for correlation of potential energy surface well depths with energy transfer dynamics at the gas-surface interface. When the methyl mimic is used as a baseline for the trends in energy transfer dynamics, the theoretical calculations can be used to predict the trends seen on the polar surfaces.

Overall, this research has helped in creating a deeper understanding of reaction mechanisms via energy transfer dynamics. This research has helped to establish a method that could potentially be used in the future to estimate trends in gas surface scattering.

References

1. Gray, H. A.; Cass, G. R.; Huntzicker, J. J.; Hyerdahl, E. K.; Rau, J. A., Characteristics of Atmospheric Organic and Elemental Carbon Particle Concentrations in Los-Angeles. *Environmental Science and Technology* **1986,** 20, 580.
2. Murphy, D. M.; Thomson, D. S.; Mahoney, T. M. J., In situ measurements of organics, meteritic material, mercury, and other elements in aerosols at 5 to 19 kilometers. *Science* **1998,** 282, 1664.
3. Novakov, T.; Penner, J. E., Large contribution of organic aerosols to cloud-condensation-nuclei concentrations. *Nature* **1993,** 365, (6449), 823-826.
4. Blando, J. D.; Porcja, R. J.; Li, T. H.; Bowman, D.; Lioy, P. J.; Turpin, B. J., Secondary Formation and the Smoky Mountain Organic Aerosol: An Examination of Aerosol Polarity and Functional Group Composition During SEAVS. *Environmental Science and Technology* **1998,** 32, (5), 604-613.
5. Claeys, M.; Wang, W.; Ion, A. C.; Kourtchev, I.; Gelencser, A.; Maenhaut, W., Formation of secondary organic aerosols from isoprene and its gas-phase oxidation products through reaction with hydrogen peroxide. *Atmospheric Environment* **2004,** 38, (25), 4093-4098.
6. Hoffmann, T.; Odum, J. R.; Bowman, F.; Collins, D.; Klockow, D.; Flagan, R. C.; Seinfeld, J. H., Formation of Organic Aerosols from the Oxidation of Birogenic Hydrocarbons. *Journal of Atmospheric Chemistry* **1997,** 26, (2), 189-222.
7. Jang, M.; Czoschke, N. M.; Northcross, A. L., Atmospheric organic aerosol production by heterogeneous acid-catalyzed reactions. *Chemical Physics Physical Chemistry* **2004,** 5, (11), 1647-1661.
8. Saxena, P.; Hildemann, L. M., Water-soluble organics in atmospheric particles: A critical review of the literature and application of thermodynamics to identify candidate compounds. *Journal of Atmospheric Chemistry* **1996,** 24, (1), 57-109.
9. Saecker, M. E.; Nathanson, G. M., Collisions of protic and aprotic gases with hydrogen bonding and hydrocarbon liquids. *Journal of Chemical Physics* **1993,** 99, (9), 7056-7068.
10. Benjamin, I.; Wilson, M. A.; Pohorille, A.; Nathanson, G. M., Scattering of water from the glycerol liquid-vacuum interface. *Chemical Physics Letters* **1995,** 243, (3-4), 222-228.
11. Lawrence, J. R.; Glass, S. V.; Nathanson, G. M., Evaporation of Water through Butanol Films at the Surface of Supercooled Sulfuric Acid. In 2005; Vol. 109, pp 7449-7457.
12. Shi, Q.; Li, Y. Q.; Davidovits, P.; Jayne, J. T.; Worsnop, D. R.; Mozurkewich, M.; Kolb, C. E., *Isotope Exchange for Gas-Phase Acetic Acid and Ethanol at Aqueous Interfaces: A Study of Surface Reactions*. 1999; Vol. 103, p 2417-2430.
13. Bertilsson, L.; Potje-Kamloth, K.; Liess, H. D.; Liedberg, B., *On the Adsorption of Dimethyl Methylphosphonate on Self-Assembled Alkanethiolate Monolayers: Influence of Humidity*. 1999; Vol. 15, p 1128-1135.
14. Day, B. S.; Davis, G. M.; Morris, J. R., The effect of hydrogen-bonding and terminal group structure on the dynamics of Ar collisions with self-assembled monolayers. *Analytica Chimica Acta* **2003,** 496, 249-258.
15. Day, B. S.; Shuler, S. F.; Ducre, A.; Morris, J. R., The dynamics of gas-surface energy exchange in collisions of Ar atoms with ω-functionalized self-assembled monolayers. *Journal of Chemical Physics* **2003,** 119.

16. Lohr, J. R.; Day, B. S.; Morris, J. R., Scattering, Accommodation, and Trapping of HCl in Collisions with a Hydroxylated Self-Assembled Monolayer. *Journal of Physical Chemistry B* **2005**.
17. Valiokas, R.; Ostblom, M.; Svedhem, S.; Svensson, S. C. T.; Liedberg, B., *Thermal Stability of Self-Assembled Monolayers: Influence of Lateral Hydrogen Bonding*. 2002; Vol. 106, p 10401-10409.
18. Vogt, A. D.; Beebe, T. P., Jr., Interactions of alcohols with hydroxyl- and methyl-terminated self-assembled monolayer surfaces studied by temperature-programmed desorption. *Journal of Physical Chemistry B* **1999,** 103, (40), 8482-8489.
19. Lohr, J. R.; Day, B. S.; Morris, J. R., Dynamics of HCl Collisions with Hydroxyl- and Methyl- Terminated Self-Assembled Monolayer. *Journal of Physical Chemistry A* **2005**.
20. Chen, S.; Li, L.; Boozer, C. L.; Jiang, S., Controlled Chemical and Structural Properties of Mixed Self-Assembled Monolayers of Alkanethiols on Au(111). *Langmuir* **2000,** 16, (24), 9287-9293.
21. Dubois, L. H.; Nuzzo, R. G., Synthesis, structure, and properties of model organic surfaces. *Annual Review of Physical Chemistry* **1992,** 43, 437-63.
22. Li, L.; Chen, S.; Jiang, S., Molecular-Scale Mixed Alkanethiol Monolayers of Different Terminal Groups on Au(111) by Low-Current Scanning Tunneling Microscopy. *Langmuir* **2003,** 19, (8), 3266-3271.
23. Troughton, C.; Tao, Y.-T.; Evall, J.; Whitesides, G. M.; Nuzzo, R. G., Formation of Monolayer Films by the Spontaneous Assembly of Organic Thiols from Solution onto Gold. *Journal of the American Chemical Society* **1989,** 111, 321-335.
24. Ulman, A., Formation and Structure of Self-Assembled Monolayers. In 1996; Vol. 96, pp 1533-1554.
25. Auerbach, D. J., *Atomic and Molecular Beam Methods*. Oxford University Press: New York, 1988; Vol. 1.
26. Fiehrer, K. M.; Nathanson, G. M., Energy and Angle-Resolved Uptake of Organic Molecules in Concentrated Sulfuric Acid. *Journal of the American Chemical Society* **1997,** 119, 251.
27. Klassen, J. K.; Fiehrer, K. M.; Nathanson, G. M., Collisions of Organic Molecules with Concentrated Sulfuric Acid: Scattering, Trapping, and Desorption. **1997,** 101, (44), 9098-9106.
28. Klassen, J. K.; Nathanson, G. M., Hydrogen-Bond Breaking and Proton Exchange in Collisions of Gaseous Formic Acid with Liquid Sulfuric Acid. *Science* **1996,** 273, 333-335.
29. Morris, J. R.; Behr, P.; Antman, M. D.; Ringeisen, B. R.; Splan, J.; Nathanson, G. M., Molecular Beam Scattering from Supercooled Sulfuric Acid: Collisions of HCl, HBr, and HNO_3 with 70 wt D_2SO_4. *J. Phys. Chem. A* **2000,** 104, (29), 6738-6751.
30. Ringeisen, B. R.; Muenter, A. H.; Nathanson, G. M., Collisions of HCl, DCl, and HBr with Liquid Glycerol: Gas Uptake, D -- H Exchange, and Solution Thermodynamics. *J. Phys. Chem. B* **2002,** 106, (19), 4988-4998.
31. Ringeisen, B. R.; Muenter, A. H.; Nathanson, G. M., Collisions of DCl with Liquid Glycerol: Evidence for Rapid, Near-Interfacial D--H Exchange and Desorption. In 2002; Vol. 106, pp 4999-5010.
32. Barker, J. A.; Auerbach, D. J., Gas-surface interactions and dynamics; thermal energy atomic and molecular beam studies. *Surface Science Reports* **1985,** 4, (1-2), 1-99.
33. Nathanson, G. M., Molecular beam studies of gas-liquid interfaces. *Annual Review of Physical Chemistry* **2004,** 55, 231-255.

34. Rettner, C. T.; Auerbach, D. J., Probing the dynamics of gas-surface interactions with high-energy molecular beams. *Comments on Atomic and Molecular Physics* **1987,** 20, (3), 153-69.
35. Day, B. S.; Morris, J. R., Even-Odd Orientation and Chain-Length Effects in the Energy Exchange of Argon Collisions with Self-Assembled Monolayers. *J. Phys. Chem. B* **2003,** 107, (29), 7120-7125.
36. Day, B. S.; Morris, J. R., Packing density and structure effects on energy-transfer dynamics in argon collisions with organic monolayers. *The Journal of Chemical Physics* **2005,** 122, 234714.
37. King, M. E.; Saecker, M. E.; Nathanson, G. M., The thermal roughening of liquid surfaces and its effect on gas--liquid collisions. *The Journal of Chemical Physics* **1994,** 101, (3), 2539-2547.
38. Nuzzo, R. G.; Dubois, L. H.; Allara, D. L., Fundamental Studies of Microscopic Wetting on Organic Surfaces. 1. Formation and Structural Characterization of a Self-Consistent Series of Polyfunctional Organic Monolayers. *Journal of American Chemical Society* **1990,** 112, 558-569.
39. Porter, M. D.; Bright, T. B.; Allara, D. L.; Chidsey, C. E. D., Spontaneously organized molecular assemblies. 4. Structural characterization of n-alkyl thiol monolayers on gold by optical ellipsometry, infrared spectroscopy, and electrochemistry. *Journal of the American Chemical Society* **1987,** 109, (12), 3559-68.
40. Greenler, R. G., Infrared Study of Adsorbed Molecules on Metal Surfaces by reflection Techniques. *The Journal of Chemical Physics* **1966,** 44, (1), 310-315.
41. Yan, T.; Isa, N.; Gibson, K. D.; Sibener, S. J.; Hase, W. L., Role of Surface Intramolecular Dynamics in the Efficiency of Energy Transfer in Ne Atom Collisions with a Hexylthiolate Self-Assembled Monolayer. *J. Phys. Chem. A* **2003,** 107, (49), 10600-10607.
42. King, M. E.; Nathanson, G. M.; Hanning-Lee, M. A.; Minton, T. K., Probing the Microscopic Corrugation of Liquid Surfaces with Fas-Liquid Collisions. *Physical Review Letters* **1993,** 70, (7), 1026-1029.
43. Rettner, C. T.; Auerbach, D. J.; Tully, J. C.; Kleyn, A. W., Chemical Dynamics at the Gas-Surface Interface. In 1996; Vol. 100, pp 13021-13033.
44. Dubois, L. H.; Zegarski, B. R.; Nuzzo, R. G., Fundamental studies of the interaction of adsorbates on organic surfaces. *Proceedings of the National Academy of Sciences of the United States of America* **1987,** 84, 4739-4742.
45. Perkins, B. G.; Nesbitt, D. J., Quantum-state-resolved CO2 scattering dynamics at the gas-liquid interface: Incident collision energy and liquid dependence. *Journal of Physical Chemistry B* **2006,** 110, (34), 17126-17137.
46. Ben-Naim, A.; Marcus, Y., Solvation thermodynamics of nonionic solutes. *The Journal of Chemical Physics* **1984,** 81, (4), 2016-2027.
47. *International Union of Pure and Applied Chemistry Solubility Data Series*. Pergamon: New York, 1979-1989; Vol. 1 (Ne), 21 (NH_3), 27-28 (CH_4), 37-38 (H_2O).
48. Gmehling, J.; Onken, U.; Arlt, W., *Vapor-Liquid Equilibrium Data Collection Aqueous-Organic Systems: Chemistry Data Series*. Dechema: Frankfurt, 1981; Vol. 1, p 46-63.
49. M. J. Frisch, G. W. T., H. B. Schlegel, G. E. Scuseria, M. A. Robb, J. R. Cheeseman, J. A. Montgomery, Jr., T. Vreven, K. N. Kudin, J. C. Burant, J. M. Millam, S. S. Iyengar, J. Tomasi, V. Barone, B. Mennucci, M. Cossi, G. Scalmani, N. Rega, G. A. Petersson, H. Nakatsuji, M. Hada, M. Ehara, K. Toyota, R. Fukuda, J. Hasegawa, M. Ishida, T. Nakajima, Y.

Honda, O. Kitao, H. Nakai, M. Klene, X. Li, J. E. Knox, H. P. Hratchian, J. B. Cross, V. Bakken, C. Adamo, J. Jaramillo, R. Gomperts, R. E. Stratmann, O. Yazyev, A. J. Austin, R. Cammi, C. Pomelli, J. W. Ochterski, P. Y. Ayala, K. Morokuma, G. A. Voth, P. Salvador, J. J. Dannenberg, V. G. Zakrzewski, S. Dapprich, A. D. Daniels, M. C. Strain, O. Farkas, D. K. Malick, A. D. Rabuck, K. Raghavachari, J. B. Foresman, J. V. Ortiz, Q. Cui, A. G. Baboul, S. Clifford, J. Cioslowski, B. B. Stefanov, G. Liu, A. Liashenko, P. Piskorz, I. Komaromi, R. L. Martin, D. J. Fox, T. Keith, M. A. Al-Laham, C. Y. Peng, A. Nanayakkara, M. Challacombe, P. M. W. Gill, B. Johnson, W. Chen, M. W. Wong, C. Gonzalez, and J. A. Pople, *Gaussian 03, Revision C.02*, Gaussian Inc.: Wallingford, CT, 2004.

50. Alexander, W. A., *(private communication)*.